Experimental study on the feasibility of microwave heating fracturing for enhanced shale gas recovery

Tianyu Chen [a], Xu Zheng [b], Xin Qiu [a], Xia-Ting Feng [a,*], Derek Elsworth [c], Guanglei Cui [a,**], Zhanhe Jia [a], Zhejun Pan [d]

[a] *Key Laboratory of Ministry of Education on Safe Mining of Deep Metal Mines, Northeastern University, Shenyang, 110004, China*
[b] *Department of Civil Engineering, Liaoning Technical University, Fuxin, 123000, China*
[c] *Department of Energy and Mineral Engineering, EMS Energy Institute and G3 Center, Pennsylvania State University, University Park, PA, 16802, USA*
[d] *CSIRO Energy Business Unit, Private Bag 10, Clayton South, VIC, 3169, Australia*

ARTICLE INFO	ABSTRACT
Keywords: Microwave fracturing Thermal-induced fracture High stress Permeability Compressibility	Microwave heating fracturing is potentially a green stimulation technology for gas shale recovery. However, the mechanism together with permeability evolution of microwave irradiated reservoir remain unclear. To fill this knowledge gap, the responses of Longmaxi shale from the Sichuan Basin, southwest China, to both continuous and intermittent microwave stimulation along variable microwave heating paths were explored. A complex thermally-induced fracture network can be formed gradually without sudden collapse under intermittent microwave irradiation. Changes in the petrophysical parameters of the shale including wave velocity, weight and volume at different intermittent microwave irradiation steps were measured together with temperature variation. The evolution of permeabilities for the two shale samples with alternately parallel and vertical beddings at different effective stresses was analyzed both before and after microwave irradiation. After the last step of intermittent microwave irradiation in this study, the shale permeability increased by two to four orders of magnitude for the shale sample with flow parallel to bedding and one to two orders of magnitude with flow perpendicular to bedding. Microwave treatment accentuates the anisotropy between bedding-parallel and bedding-normal permeabilities. Evolving pore size was measured by high-pressure mercury porosimetry and thermal-induced fracture characteristics and the changes of mineral composition were characterized by SEM combined with Energy Dispersive Spectroscopy (EDS). Thermally- and chemically-induced swelling stresses are mainly responsible for the development of fractures and micro-porosity in the shale. A permeability model with variable compressibility coefficient was adopted to fit the experimental data for shale permeability across a wide range of effective stresses from 2.5 MPa to 59.5 MPa. Shale fracture compressibility decreases in the later stage of microwave irradiation, suggesting the hardening of thermal-induced fractures.

1. Introduction

Commercial production of shale gas is mainly achieved through the applications of horizontal drilling and hydraulic fracturing technologies (Boudet et al., 2014). However, hydraulic fracturing not only consumes large volumes of potentially potable water resources but also potentially causes soil and water pollution and other environmental problems. Much more importantly, after hydraulic fracturing, the flowback ratio of the fracturing fluid is very low, with ~50–90% of the fracturing fluid retained in the reservoir (Wang et al., 2019a) and trapped in water-wet

pores (Xu et al., 2016). These retained water would impair gas flow and reduce gas production rate (Cui et al., 2020b). Microwave fracturing is considered to be a green waterless fracturing technology that can be widely used in unconventional gas/oil reservoirs (Li et al., 2019; Liu et al., 2020; Yang et al., 2017) which can rapidly heat shale formations without contact or convection (Cui et al., 2020a). Due to the heterogeneity of the mineral distribution within the reservoir, the temperature distribution within the rock mass is heterogeneous resulting in a heterogeneous distribution of thermal stresses at the grain-scale and the potential for thermal fracturing (Seehra et al., 2007). The reduced

---

permeability due to water retention can be largely recovered by treatment at high temperatures (Zhang et al., 2015). Furthermore, microwave-induced thermal fracturing also has the potential to accelerate desorption and diffusion of methane in the adsorbed state, take up to 20%–85% of the total gas (Chen et al., 2015b; Cui et al., 2020c), and thereby enhance ultimate gas recovery (Liu et al., 2018). Thus, the combination of hydraulic fracturing and microwave heating stimulation may effectively deal with formation damage resulting from water blockage and clay swelling.

Mineral composition of rocks can be altered by microwave-induced high temperatures and related reactive transformations (Flesoura et al., 2019; Jones, 2005). For instance, clay minerals can be dehydrated, degraded or decomposed (Kang et al., 2016). Besides that, under microwave irradiation, when the thermal stress within the irradiated region exceeds the strength of the mineral particles or cement, intergranular and transgranular fractures may appear and such damage can be indicated by changes in the acoustic wave velocity of the rock (Zheng et al., 2017). Expansion of pores and the creation of fractures will impact both porosity and associated permeability of the rock, potentially increasing the permeability by orders of magnitude (Wang et al., 2016).

Lots of experiment works are conducted to investigate the microstructure variations of reservoir rock before and after microwave heating (Li et al., 2016). It is found that (1) micro-fractures become prominent after microwave heating (Chen et al., 2018; Sahoo et al., 2011) and both inter-granular and trans-granular fracture would appear (Jones et al., 2007); (2) new crosslinking surfaces were created in the closed pores thus increasing particle size (Zhou et al., 2015); and surface area and total and pore volume increase while the average pore diameter would increase (Liu et al., 2015) or decrease (Ge et al., 2013) and (3) both matrix and fracture permeability were measured with an increase of more than three orders of magnitude (Chen et al., 2018, 2021a). Numerical models were also established to study microwave heating effect. In the early work, 2-D models were firstly established to study the electromagnetic and thermal field distribution of reservoir rock and the impacts of microwave power, frequency and irradiation time (Wang and Djordjevic, 2014; Meisels et al., 2015). While these models were simplified because of the limitation of computing time. Later 3-D models were proposed with the framework of COMSOL Multiphysics (Cui et al., 2020a; Li et al., 2019) and ANSYS (Wang et al., 2017). COMSOL has a powerful ability in simulating microwave heating process while it cannot handle large scale models because of the RAM limitation (Salvi et al., 2010). On the contrary, ANSYS can handle large scale problem but more complicated operations are needed (Salvi et al., 2010; Wang et al., 2015).

The application of the microwave to the unconventional reservoir has been discussed since the patent 'Oil well microwave tools' (Kasevich, 2008). In the heavy oil industry, the thermally enhanced oil recovery methods are widely applied (Rui et al., 2018). Inspired from this, microwave was proposed to heat the oil reservoir thus reducing its viscosity and promoting oil flow (Bientinesi et al., 2013; Mutyala et al., 2010). Based on these experiences, conceptual designs of on-site microwave heating system for unconventional gas reservoir were proposed for shale gas or coalbed methane (Hong et al., 2016; Liu et al., 2018) with both the horizontal and vertical well applicable (Li et al., 2016; Liu et al., 2018).

Even there are abundant experimental observations and modeling analyses defining the impacts of microwave irradiation, several knowledge gap remain: (i) most previous works took their attention on coal (Li et al., 2019) and oil shale (Yang et al., 2017) while the response of gas shales to microwave heating will be different from that of coal and oil shale. Compared with coal, the brittle mineral content in gas shales is higher and the organic carbon content is lower (Wang et al., 2019b; Youjun 2017). Compared with oil shale, gas shales generally lack liquid oil within the matrix; (ii) the limited research work paid attention to the variations in flow transport ability induced by the microwave irradiation (Liu et al., 2018; Zhu et al., 2016). Even the mechanism of the fracture

induced by saturated vapor pressure in tight rock matrix are widely investigated in the study of Chen et al. (2018, 2021a) and that induced by differential thermal stress between distinct minerals is rare studied; (iii) Understanding and evaluating the evolution of permeability resulting from microwave-induced fracturing under high effective stress is the key in evaluating the potential of microwave fracturing to influence gas production because that the effective stress of some deep-buried shale gas reservoirs can be as high as 100 MPa (Chen et al., 2019; Cui et al., 2018). Therefore it is concluded that (i) more experimental studies of microwave heating fracturing are necessary to constrain the true impacts of variations in petrophysical properties, pre-existing permeability and pore structure of real gas shales on the true evolution of porosity and permeability; and (ii) characterizing fracturing behaviour and the resulting variation in permeability of microwave-fractured shale at high stresses is therefore crucial to extend this technique to shale gas production.

In this paper, the impacts of microwave heating paths in the generation of complex thermally-induced fractures were explored. The evolution of rock physical properties during microwave stimulation was also investigated. The evolution of permeability of microwave-fractured shales, treated for a spectrum of microwave exposure times, was examined under a wide range of effective stresses (from 1.5 MPa to 59.5 MPa). The effects of microwave stimulation on pore and fracture structure were characterized by high-pressure mercury injection porosimetry and scanning electron microscopy (SEM). The effects of microwave irradiation on the resulting compressibility and permeability were linked to define the evolution of stress/deformation-dependent transport characteristics. The anisotropy of shale permeability following microwave-treatment was also studied.

2. Experimental

2.1. Samples

The shale used in this study was collected from an outcrop of the Silurian Longmaxi formation of the Sichuan Basin in southwest China. Fresh shale blocks were selected to drill the samples of three sizes, 5 cm in diameter and 2.5, 7.5 cm and 10 cm in height. Offcuts were used for the measurement of the organic carbon content, maturity and mineral composition. The geochemical properties of the shale are summarized in Table 1.

2.2. Experiment methods

In order to eliminate the influence of moisture content as an uncontrolled variable on the effects of microwave heating fracturing, all samples were dried under vacuum for more than 72 h before the experiments. A household microwave oven (Galanz, G70F20CN1L-DG (B0), Fig. A.1) with a constant power of 700 W was used for irradiation and heating of the shale samples. The internal space of the microwave oven is 329 mm × 315 mm × 180 mm. The waveguide is located at the top of the right side in the microwave oven with a dimension of 50 mm × 50 mm × 70 mm. Shale samples in the three sizes were used to study the size effect on microwave fracturing. The lengths of the three samples are 25, 75 and 100 mm, respectively. This represents volumes in multiples of 1x, 3x and 4x, with anticipated inversely-correlated impacts of heating. The initiation and propagation of fractures induced by microwave heating were selected as studied.

2.2.1. Preferred heating path determination

To determine the preferred heating path of microwave irradiation, two types of microwave heating paths were investigated: the first heating path included continuous microwave irradiation (CMI) and the second intermittent microwave irradiation (IMI). During the process of intermittent microwave irradiation, the magnetron in the microwave oven is applied in bursts of 20 s on then 10 s off, compared to the

Table 1

Geochemical properties of the shale samples.

Mineral compositions (%)							TOC (%)	$R_{o,max}$ (%)
Quartz	Feldspar	Pyrite	Clay minerals		Calcite	Dolomite		
			Illite	Chlorite				
40.62	1.45	1.74	12.23	0.25	30.46	9.96	3.29	2.51

continuous case. The microwave exposure time was increased step by step for the two microwave heating paths. Before each stage of microwave heating, the sample was preheated to 90 °C by low-level microwave irradiation to simulate the in-situ reservoir temperature. After the microwave irradiation was applied for the first time step, the sample was taken out of the microwave oven and the temperature was slowly lowered to 90 °C (simulating a return to reservoir temperature). Then the next microwave irradiation step is performed, and the time of microwave heating in the next step was 30 s longer than that in the previous step.

Before and after each microwave heating step, the temperature of the sample was determined by a Fluke infrared thermometer (model: 568–2) with an accuracy of ±1 °C; the weight of the sample was measured by a Mettler Toledo balance (model: MS1602TS) with an accuracy of 0.01 g; the dimension of the sample was measured with a vernier caliper to analyze its volumetric change; and the wave velocity of the sample was measured using a Proceq wave velocity meter. It should be noted that after microwave treatment, the mass, volume and wave velocity of the sample were measured when the temperature was reduced to 90 °C. The results of the microwave-induced fracturing under the two different heating paths were compared and analyzed. The microwave heating path with the preferred resulting microwave fracturing network was then selected to investigate the effect of exposure microwave time on permeability.

2.2.2. Variations of permeability and micro-structure

Before microwave heating, the permeabilities of shale samples, with the diameter of 5 cm in diameter and length of 10 cm in height, with both flow-parallel and flow-perpendicular to bedding were measured under different effective stresses. Then, the shale samples were subjected to microwave heating to follow the preferred heating path. After microwave stimulation, the permeabilities of the shale samples were measured again. The transient pulse method is applied to measure permeability proposed by Brace et al. (1968). The own designed multi-physics coupling testing system was used for permeability measurement with schematic diagram shown in Fig. A.2. The details of the triaxial pressure chamber and stress loading procedures of the experimental setup used for the permeability measurement have been described in our previous work (Chen et al., 2019). The measuring accuracy and the range of the pressure sensors is 0.01% of the full scale (FS) and 0–20 MPa, respectively. A Keller differential pressure transducer is added to monitor the gas pressure difference between the upstream and downstream gas cylinders with measuring range and accuracy of 0–1 MPa and 0.1% FS (Chen et al., 2019). The upstream and downstream cylinders were full of gases but with different gas pressures, therefore a gas pressure difference exists between the two cylinders. The permeability is calculated as:

$$\frac{(P_u - P_d)}{(P_{u,0} - P_{d,0})} = e^{-\alpha t} \qquad (1)$$

where P denotes the gas pressure, the subscript u and d represent the gas pressures in the upstream and downstream cylinders at the testing time t, and the subscript 0 denotes the initial state. α is a parameter representing the pressure decay exponent, written as (Brace et al., 1968; Tan et al., 2018):

$$\alpha = \frac{kA(P_{u,0} + P_{d,0})}{2\mu L}\left(\frac{1}{V_u} + \frac{1}{V_d}\right) \qquad (2)$$

in which k denotes the measured permeability value, A denotes the area of the sample end face, L defines the sample length, μ denotes the fluid viscosity, V_u and V_d are the volumes of the upstream and downstream cylinders (inclusive of tubing), respectively.

Helium was used as the permeant in the permeability tests. After sample installation, the gas injection system and the shale sample were evacuated for more than 72 h to ensure that the contamination induced by air is fully eliminated. Hydrostatic pressure was then applied with a constant loading rate at 1 MPa/min. The hydrostatic effective stress for the permeability experiments was enhanced from 1.5 MPa to 59.5 MPa in ten increments of confining pressure. The gas pressure used to determine the permeability was 0.5 MPa. In order to consolidate the sample, after the permeability measurement of the first loading cycle, the permeability of the shale sample was measured again following the application of the same loading path.

The fracture characteristics and any variations in the mineral composition that evolved on the surface of the heating-induced fracture were measured by Scanning Electron Microscopy (SEM) and Energy Dispersive Spectroscopy (EDS). In this work, Scanning electron microscope (TESCAN MIRA 3 XMU) is applied (Fig. A.3). The shale samples, both before and after microwave irradiation, were polished by argon ion beam, and the changes in pore structure and mineral composition in the shale under the microwave treatment were observed by SEM and EDS. Pore size distribution and volume of the shale samples before and after microwave treatment were measured by high-pressure mercury injection porosimetry. The experimental procedure is shown in Fig. 1.

3. Results

3.1. Change in petrophysical properties

Fig. 2 shows the variation in temperature for the shale samples of different sizes under different microwave heating paths. For samples 2, 4 and 6 with lengths of 25 mm, 75 mm and 100 mm, respectively, the maximum microwave-induced temperature under intermittent microwave irradiation is 550 °C, 422 °C and 437 °C, respectively. The smaller the sample, the higher the temperature rise rate at the same duration of microwave exposure.

After microwave treatment for 600 s, the temperatures of sample 5 (CMI) and sample 6 (IMI) reached 394 °C and 305 °C, respectively. Fig. 2 also illustrates the dependence of temperature with microwave irradiation time for the shale samples with a length of 100 mm under intermittent microwave irradiation. In the initial stage of microwave treatment, the surface temperature of the shale samples increases rapidly with the progress of microwave heating time but then slows down, reaching a plateau of near-constant temperature. The temperature plateaus may be related to the phase transition of minerals or evaporation of bound water with details discussed in Section 4.1. The increase in temperature with the microwave exposure time for different shale samples of the same size and mass, shows good consistency.

The shale samples under continuous microwave irradiation rapidly disintegrated the following exposure for 20 min (Fig. 3). Continuous microwave irradiation readily leads to a rapid rise in temperature of
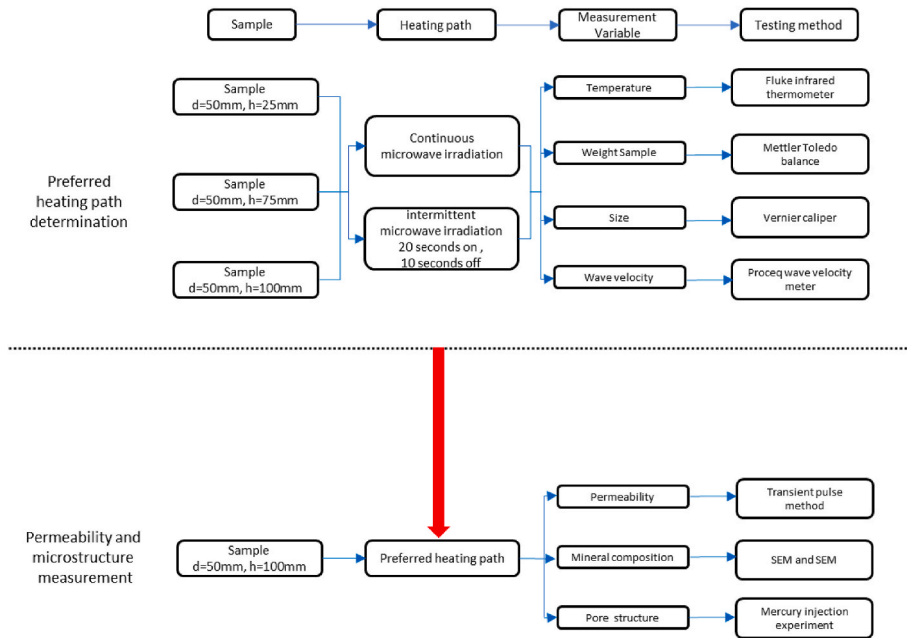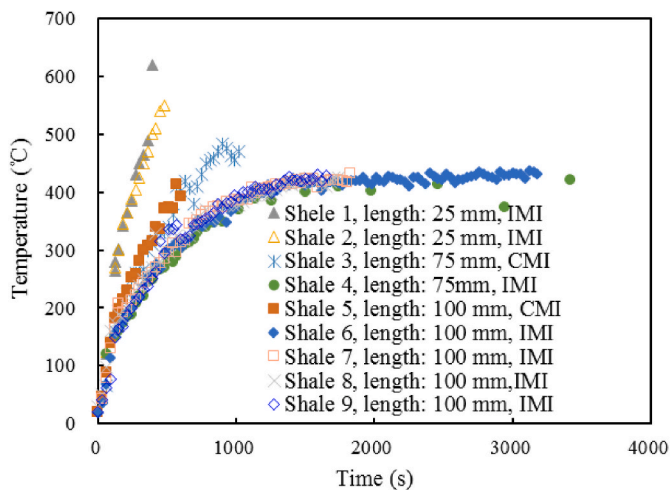
Fig. 1. Experimental procedures.

Fig. 2. Temperature changes with microwave heating time for shale samples.


Fig. 3. Effects on shale samples of continuous microwave treatment.

sensitive minerals, resulting in the rapid accumulation of thermal-stress in the shale samples. Simultaneously, the rapid accumulation of gas generated by microwave-induced chemical reaction of the minerals can also result in a sharp increase in gas pressure. The concentration of thermal-stress and the failure to drain the gas and to release gas pressure in the tight shale sample eventually caused a sudden collapse. Heating-induced fractures gradually developed in the shale sample at different steps in the second intermittent microwave heating path and the sample remained intact without disintegration. In the process of intermittent stepwise microwave stimulation, the heating-induced fracture generated in the previous microwave irradiation step allows the release of thermal stress and the gas in the next step, thus avoiding the concentration of internal stress and gas pressure. In order to ensure wellbore stability during microwave fracturing, the second microwave heating path was selected as the preferred microwave irradiation path for further study.

Fig. 4 displays the dependence of weight, volume and acoustic wave velocity with temperature of the shale samples for each microwave heating step. It should be noted that the temperature on the horizontal axis refers to the highest temperature of the sample after corresponding microwave. Weight reduction in the shale samples was observed during the process of microwave treatment. The mass loss of the shale samples is mainly due to the generation of gases from mineral chemical reactions and the evaporation of bound water under the high temperature induced by microwave treatment. The chemical reactions of minerals and related gas generation may result in the development of pores and micro-fractures in the shale. The details were discussed in Section 4.1. The mass loss of the shale samples is closely related to the microwave-induced temperature increase. When the microwave-induced temperature is below 150 °C, the mass loss of the shale samples is small. For the microwave-induced maximum temperature between 150 °C and 400 °C, loss of mass is clearly observed. Shale weight loss rate increases rapidly at temperatures higher than 400 °C, which suggests that some minerals react rapidly or water evaporates quickly in the shale at this tempera-ture. For example, after 3180 s of microwave treatment, the temperature reached 432.7 °C for sample 6 with a mass loss of 2.9%.

As apparent from Fig. 4, the volume of the shale samples increases
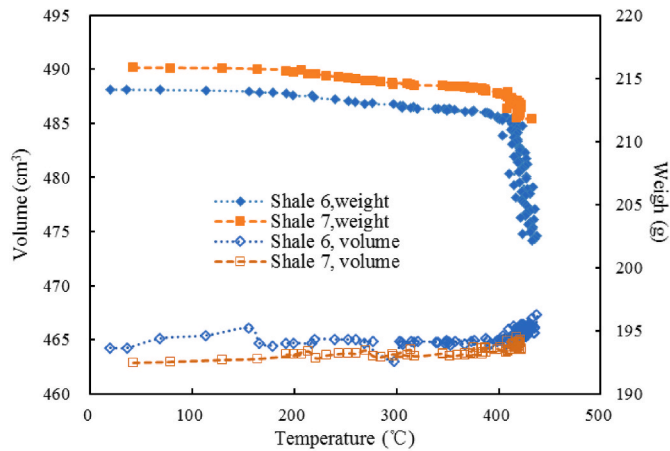
(a) Change in the weight and volume of the shale samples
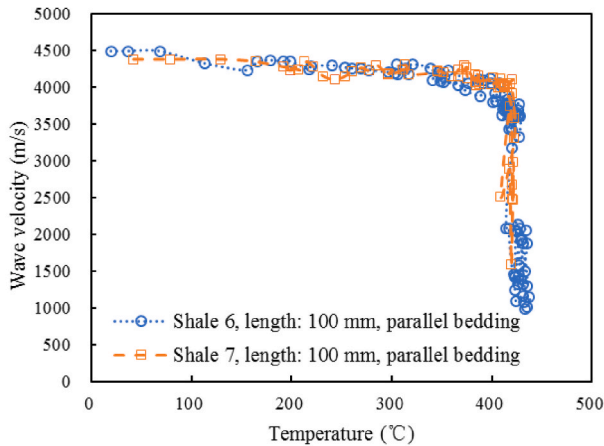
(b) Change in the acoustic wave velocity of the shale samples

Fig. 4. Change in the weight, volume and acoustic wave velocity of the shale samples with temperature under intermittent microwave irradiation.

and the acoustic wave velocity decreases with the enhanced temperature. The increase of shale sample volume and the decrease of wave velocity mainly resulted from the initiation and development of fractures induced by differential thermal stresses. The details were discussed in Section 4.2. The variation in the volume and acoustic wave velocity indicates that the severity of microwave-heating induced fracturing in the shale gradually increases with the increase of temperature. The volume increase rate and rate of decrease in the acoustic wave velocity also increase rapidly at temperatures higher than 400 °C.

3.2. Thermally-induced variation of pore structure

After an extended duration of microwave exposure, heating-induced oxidation of carbon on the fracture surface becomes more apparent and pronounced. The porosities of the original shale sample, the shale sample with shallower oxidation depth, and that with greater oxidation depth are 1.57%, 2.67% and 3.83%, respectively. The shale porosity increases with the proportion of white oxidized shale. The overall porosity of the shale did not increase significantly after microwave irradiation, which may be due to the low microwave power used in this work.

Fig. 5 shows variations in the pore area and volume for the shale samples both before and after microwave treatment. The average pore diameter of the original shale sample, the shale sample with shallow oxidation penetration depth, and that with deep oxidation penetration depth are 8.58, 8.58 and 8.27 nm, respectively. There is no difference in

the range of distribution of pore diameters in shale before and after microwave irradiation. The increase in the porosity caused by microwave irradiation mainly comes from the increase in the number of pores with a diameter less than 130 nm.

3.3. Thermally-induced fracture growth

The fractures developed at different angles of shale samples are shown following the last microwave treatment step under intermittent microwave treatment in Fig. 6 with other representative microwave treatment step shown in Fig. A.4 and Fig. A.5. The shale bedding first delaminates at lower temperatures. For most of the shale samples examined in this work, heating-induced fractures first appear along the bedding when the microwave-induced temperature is > 150 °C as shown both in Fig. A.4(a) and Fig. A.5(a). With the further application of microwave irradiation, the initiation of thermally-induced fractures perpendicular to the bedding direction can be observed as illustrated in Fig. A.4(b) and Fig. A.5(b). The fractures in the direction vertical to the bedding mostly develop along the edge of the microwave-induced fractures developed parallel to the bedding. The development of thermally-induced fractures exhibit a two-staged process. After the initial initiation of fractures induced by microwave heating, the fracture aperture is in the millimeter range and principally under the action of the thermal expansion stress. However, as the temperature of the shale samples gradually decreases, the fractures close completely. As microwave irradiation is further applied, the existing thermally-induced fractures harden, and even when the temperature drops to room temperature, the clear openness of the fractures can also be observed. Finally, after full microwave irradiation, the heating-induced fractures appear as a complex network with thermally-induced fracture along bedding as the main fracture and with those passing through the multi-layer fractures as the secondary fractures.

The results of Huang et al. (2019) show that fracture growth in coal exposed to microwave irradiation is mainly due to the expansion of surface cleats, which is similar to the development of the heating-induced fractures for the shale observed in this work. While in the work of Chen et al. (2018, 2021a), the microwave-induced fractures are generally parallel to the bedding for source rock samples with a moderate amount of pore-water after 50 s of microwave irradiation. Microwave time and the existence of water together with heating induced saturated vapor pressure are the main contributors to the difference of our findings and Chen et al.'s work (2018, 2021a). The details were discussed in Section 4.2.

3.4. The effect of microwave heating on shale permeability

Permeability ratio is defined as the ratio of shale permeability after microwave irradiation relative to that before microwave irradiation at the same effective stress. Variations in permeability and permeability ratio of the shale samples with flow both parallel and perpendicular to bedding following different microwave exposure times are shown in Fig. 7, respectively. The increase in shale permeability is positively correlated with microwave treatment time. After microwave treatment, the increase in permeability is larger for shale samples with flow parallel to bedding and less for that with flow perpendicular to bedding during the second loading cycle. After 1650s of microwave irradiation, the permeability of the shale sample with flow parallel to bedding increased by two to four orders of magnitude, however, that with flow perpendicular to bedding increased by only one to two orders of magnitude. This implies that microwave treatment mainly promotes an increase in permeability parallel to the bedding direction. A consequence of this is that microwave treatment accentuates the difference between permeability in the bedding-parallel and bedding-perpendicular directions and increases the permeability anisotropy ratio. It is worth noting that for source rock samples with a moderate amount of pore-water, microwave simulation enhanced the rock permeability by more than three orders of
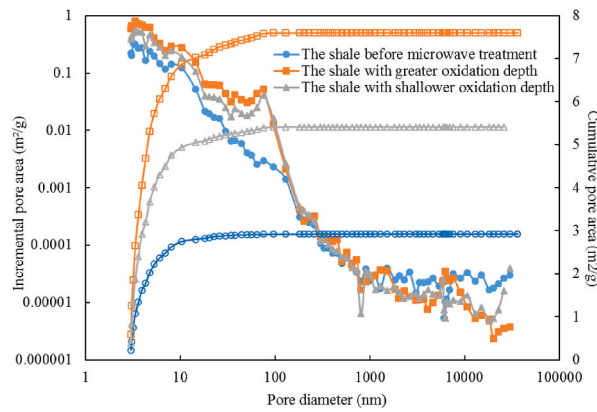
(a) Variation in the incremental pore area and cumulative pore area induced by microwave irradiation (Solid symbols: incremental pore area, Empty symbols: cumulative pore area).
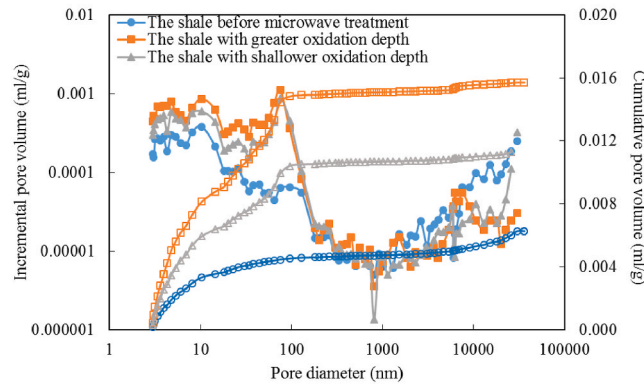
(b) Variation in incremental pore volume and cumulative pore volume induced by microwave irradiation (Solid symbols: incremental pore volume, Empty symbols: cumulative pore volume).

Fig. 5. Changes in pore structure after microwave treatment.

magnitude after 50 s of microwave irradiation under the condition of confining pressure in the study of Chen et al. (2018, 2021a). Under microwave irradiation, tight rocks with moderate water content have higher fracturing efficiency in the early stage. The details were discussed in Section 4.2.

The permeability of the shale both without and with microwave treatment decreases with an increase in stress and exhibits hysteresis in this response. When the value of effective stress is less than 10 MPa, the permeability ratio increases with an increase in the effective stress for the first loading path with a slower downward trend for the second loading path. When the value of effective stress is larger than 10 MPa, the permeability ratio shows a clear reduction. This suggests that high stress has a greater inhibiting effect on the increase of the thermally-induced fracture permeability after microwave irradiation.

Shale permeability is highly sensitive to stress. The permeability measured during the second loading cycle is used in the analysis since the shale is sufficiently consolidated to remove the major effects of hysteresis. Before microwave treatment, the permeability of the shale with flow parallel to bedding and that perpendicular to bedding at an effective stress of 59.5 MPa is 12% and 17% of that at an effective stress of 1.5 MPa, respectively. After microwave treatment for 690, 1320 and 1650 s, the permeability of the shale parallel to bedding at an effective stress of 59.5 MPa is only 1.2%, 0.35% and 0.65% of that with effective stress value of 1.5 MPa, respectively. The permeability of the shale with perpendicular to bedding at an effective stress of 59.5 MPa is only 8.9%, 2.6% and 1.6% of that at effective stress value of 1.5 MPa. The permeability of microwave heating-induced fractures is highly sensitive to stress.

The relationships between permeability measured along different bedding directions with peak microwave-induced temperature are

shown in Fig. 8. Shale permeability is positively correlated with the microwave heating-induced temperature. According to the existing data in this paper, the shale permeability increases rapidly with the enhancement in temperature with the temperature value above 325 °C, indicating that when the temperature is above a certain threshold, the fractures and pores develop rapidly.

4. Discussion

4.1. The response of mineral aggregate to the microwave in shale

Microwaves can cause atomic polarization and dipolar turning to polarization therefore stimulating dielectric reactions. When a dielectric mineral is polarized, temperature increases because of inner power dissipation of the mineral. The capacity of mineral aggregates to interact with electromagnetic waves is described by dielectric permittivity:

$$\varepsilon = \varepsilon_0(\varepsilon_r + i\varepsilon_i) \tag{3}$$

where i is the imaginary unit, ε_r is the real part of the relative permittivity, ε_i denotes the imaginary part and ε_0 defines the permittivity of a vacuum (Li et al., 2019).

For most minerals dielectric permittivity increases gradually with temperature (Jones, 2005; Flesoura et al., 2019), while some show a sudden increase with time, such as pyrite (Lovás et al., 2010). The dielectric permittivities of shale matrix contained minerals are listed in Table 2 (Aqil and Schmitt, 2010; Church et al., 1988; Josh and Clennell, 2015; Zheng et al., 2005; Zhou et al., 2011) and Fig. 9 (a) (Lovás et al., 2010) with the value of pyrite and quartz increasing with temperature and value of others treated as a constant. The specific heat capacity (C_p),
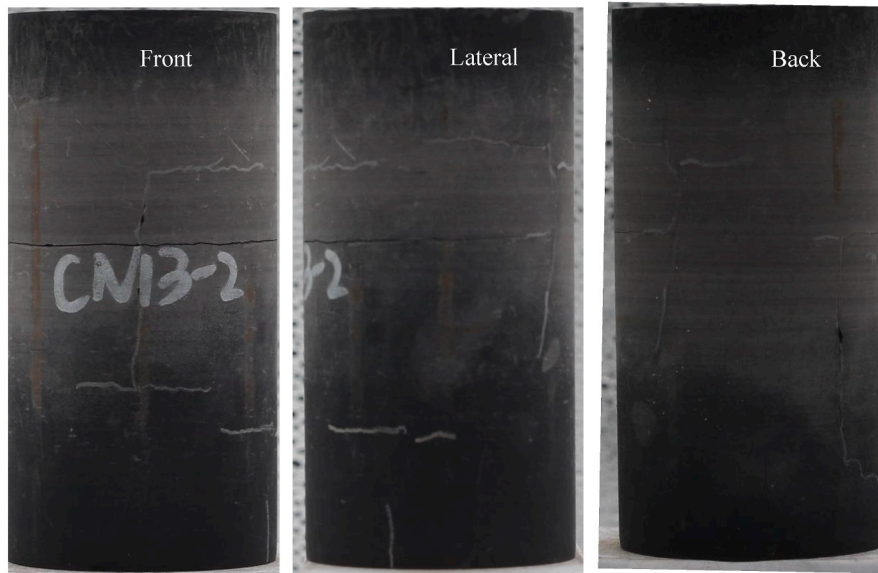
(a) Shale with flow-perpendicular bedding.
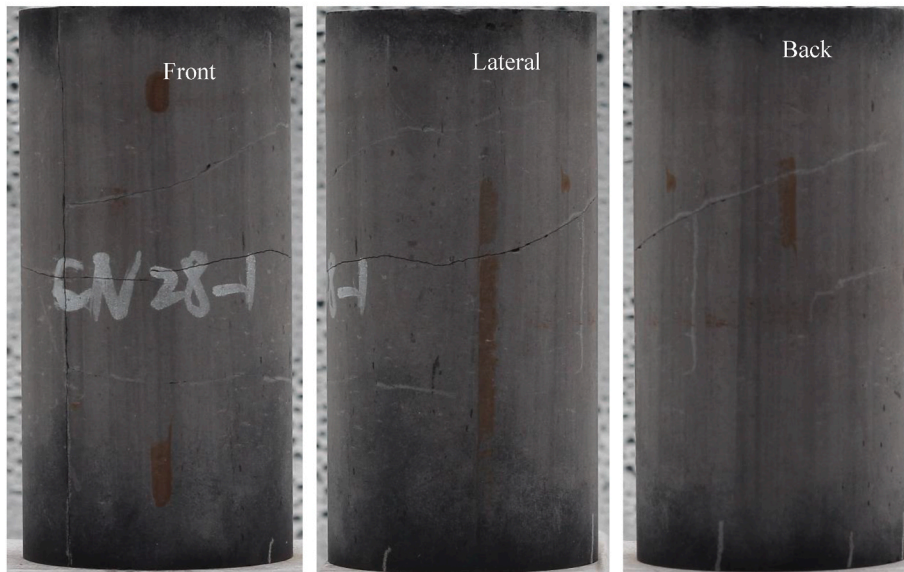
(b) Shale with flow-parallel bedding.

Fig. 6. Shale samples after intermittent microwave treatment.

defining the temperature (T) increase related to a given energy input, of shale matrix contained minerals are shown in Fig. 9 (b) (Skauge et al., 1983; Toifl et al., 2017). A peak value of the quartz due to the alpha-beta phase transition was observed.
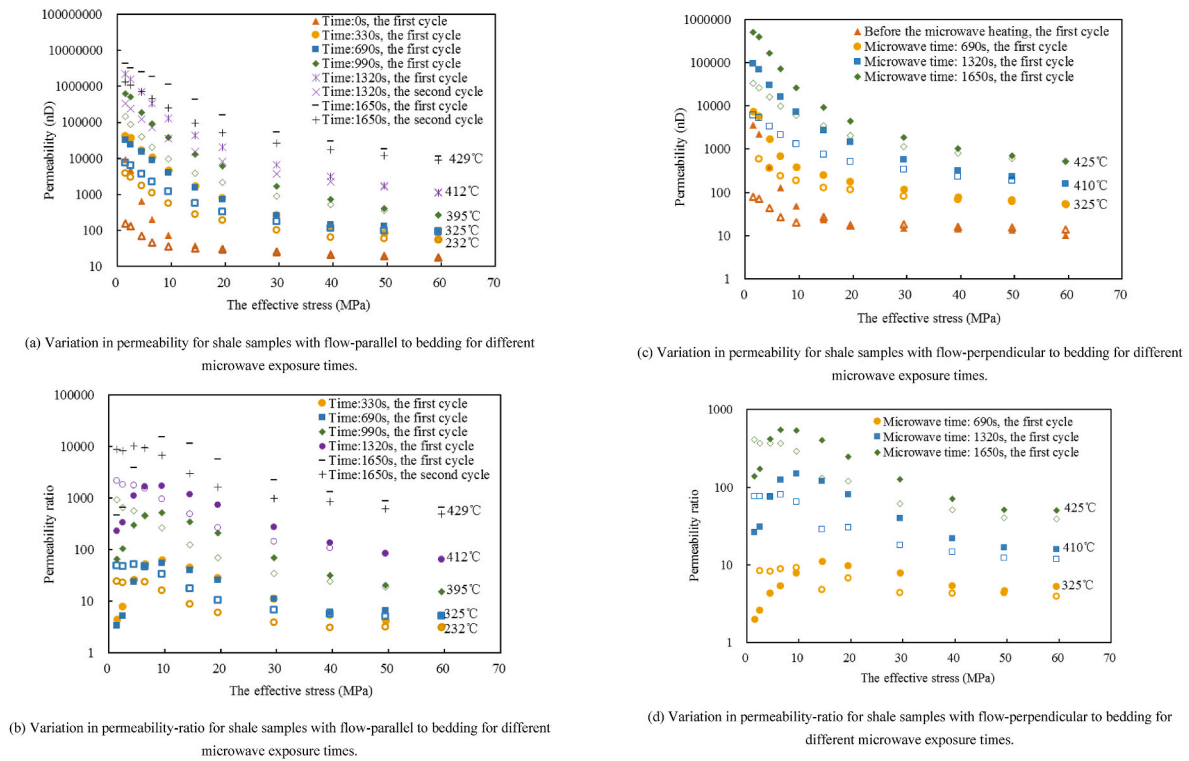
Based on the energy conservation law, the microwave absorbed energy by the mineral is equal to energy required for the temperature rise and that is (Li et al., 2019):

$$\int_{t}^{t+\Delta t} \frac{\omega \varepsilon_0 \varepsilon_i |\mathbf{E_e}|^2}{2} \mathrm{dt} = \int_{T_0}^{T_0+\Delta T} \rho_m C_p \mathrm{dT} \qquad (4)$$

where ω is the angular frequency, E_e denotes electric field, ε_r is the real part of the relative permittivity, ε_i is the imaginary part, ρ_m denotes the density of mineral and C_p defines the specific heat capacity. For a given time interval and electric field, the temperature increasing characteristic of different mineral aggregate can be obtained. The temperature rise for a constant energy input rate are highest for pyrite and clay compared to other minerals. This is a result of their larger permittivity (pyrite) and

lower specific heat capacity (clay). For the other minerals, temperature increases linearly with time in the order of dolomite (highest), then feldspar, calcite, and quartz. It should be noted that (i) for the minerals characterized with low microwave conversion capability such as calcite, and quartz, the above calculation may lead to some errors because of the ignorance of heat transfer between different minerals (ii) an induced temperature magnitude can be obtained from the small volume of the shale sample but the temperature values vary with different minerals at the micro-scale in the same area.

The temperature obtained from the sample is a macroscopic representation of the mineral temperatures at the micro-scale. In the following, each different mineral to the microwave heating are discussed. In the following work, scanning electron microscope (TESCAN MIRA 3 XMU, Fig. A3) is applied to obtain the SEM image with mineral components calibrated with Energy Dispersive Spectroscopy (EDS) Systems.

(a) Variation in permeability for shale samples with flow-parallel to bedding for different microwave exposure times.

(b) Variation in permeability-ratio for shale samples with flow-parallel to bedding for different microwave exposure times.

(c) Variation in permeability for shale samples with flow-perpendicular to bedding for different microwave exposure times.

(d) Variation in permeability-ratio for shale samples with flow-perpendicular to bedding for different microwave exposure times.

Fig. 7. Variation in permeability and permeability ratio for shale samples with flow-parallel to bedding and that flow-perpendicular to bedding for different microwave exposure times (Solid symbols: shale permeability for the first loading cycle, Hollow symbols: shale permeability for a second loading cycle).
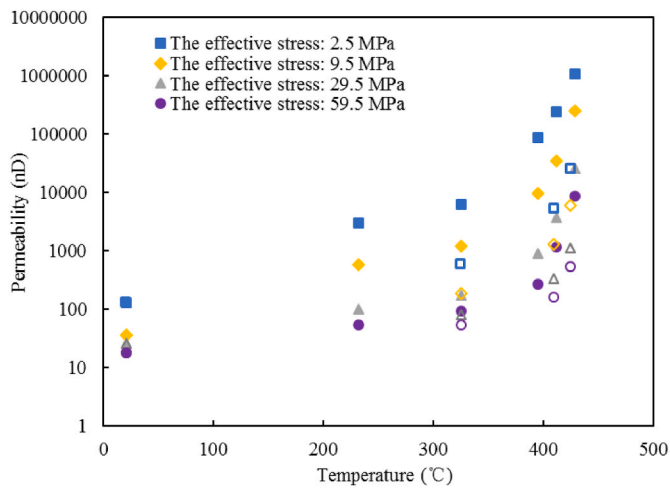
Fig. 8. Relationship between the permeability along different bedding directions of the shale relative to microwave-induced temperature (Solid symbols: shale permeability for flow-parallel to bedding, Hollow symbols: shale permeability for flow-perpendicular to bedding).

Table 2
Dielectric permittivity of the minerals in the shale samples.

	Quartz	Feldspar	Clay	Calcite	Dolomite
Real Part	3.85	5.52	4	9.2	7.41
Imaginary Part	0.0018	0.01	0.2	0.005	0.02

4.1.1. Organic matter

The microstructure and elemental distribution of the carbon enrichment area in the original and microwaved shale are presented in Fig. 10 obtained with the combination of SEM and EDS. Many nanometer-sized pores in the organic matter can be observed in the shale after microwave stimulation (Fig. 10(b)). The organic matter inside the shale can be heat up rapidly after microwave stimulation, and some kerogen rapidly absorbs heat and releases natural gas (Chen et al., 2017). When the temperature is above 400 °C, oxidation of organic matter begins to occur (Han et al., 2015). Some carbon is oxidized to release carbon dioxide (Jiang et al., 2007). Oxidation of organic matter may be one of the reasons for the rapid mass loss of shale above 400 °C (Fig. 2), with the release of gases during oxidation being responsible for the development of pores in the organic matter.

As apparent in Fig. 11(a), the crystal shape of native pyrite particles in the shale is relatively regular. The pyrite grains are dense and non-porous, and nanopores and tiny fractures develop between the native pyrite grains. However, as shown in Fig. 11(b), after microwave irradiation the pyrite framboids are broken up without obvious grain shape. As apparent in Fig. 10(a), the distribution of iron is the same as that of sulfur in the original shale. However, it can be seen from Figs. 10(b) and Fig. 11(c) that the distribution of sulfur in the microwave treated shale is similar to that of calcium in the microwaved shale. The high dielectric constant of pyrite (Lovás et al., 2010) results in its rapid oxidation to form iron oxide and release sulfur dioxide gas. Therefore, the native pyrite particles in the microwaved shale are converted into iron oxide particles. The sulfur dioxide from pyrite oxidation and the calcium oxide from calcite decomposition react at high temperature to form sulfate minerals. It can also be drawn from Fig. 11 (c) and Fig. 11 (e) that new structures are formed in some large pyrite particles after the oxidation reaction, where nanofractures and nanopores are developed.

4.1.2. Clay

Although the shale sample was dried before the experiment, the shale may still contain some connate water in the form of adsorbed water, interlay water and constitution water. The adsorbed and interlay water would be excluded at least at 100–200 °C, while 400 °C is necessary to remove constitution water in the lattice (Kang et al., 2016). Furthermore, when the temperature transits from 350 °C to 550 °C, the
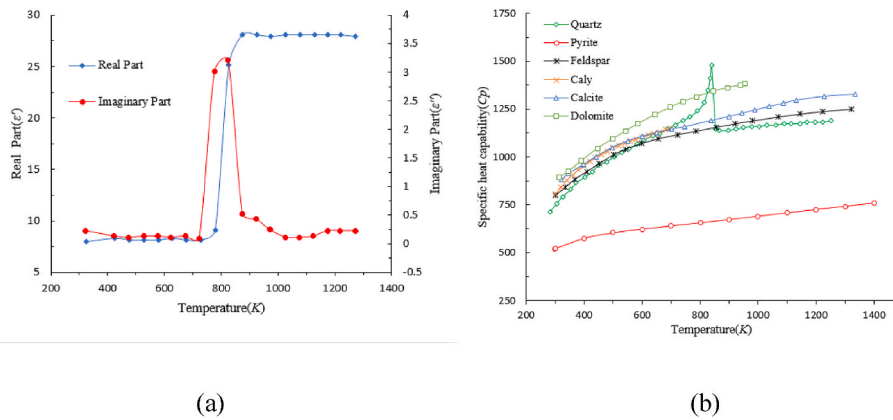
(a)   (b)

Fig. 9. Temperature-dependent (a) dielectric permittivity of pyrite (Lovás et al., 2010) and specific heat capacity of different minerals (Skauge et al., 1983; Toifl et al., 2017).

structure of illite transforms to mica (Carrol, 1970), with volume shrinkage creating new pores and microcracks (Fig. 12). During these processes, the adsorbed energy is converted to the internal energy forcing water to evaporate or mineral transform resulting the temperature plateaus observed in Fig. 2. Residual thin fragments of clay are left after this decomposition. This may be one of the reasons for the rapid increase of permeability when the microwave-induced temperature is higher than 325 °C (Fig. 8).

4.1.3. Quartz

The quartz exhibits an α-β transition at 573 °C where the trigonal a-phase changes to the hexagonal b-phase. This effect is accompanied by a significant change toward higher symmetry and volume of β-quartz, changes in specific heat capacity and volume of the unit cell (Hartlieb et al., 2016). The lower temperature α-phase has a lower symmetry and smaller volume than the higher temperature β-quartz. Although both phases can be observed on a hexagonal lattice, α-quartz has trigonal (3-fold) symmetry while β-quartz has hexagonal (6-fold) symmetry. During the phase transition process, lots of energies are needed while the temperature is kept invariable as illustrated in Fig. 2. Also a sudden increase in the specific heat capacity-temperature curve as shown in Fig. 9. Although the dielectric permittivity of quartz increase with temperature, it still in the low range. Therefore, the increase temperature in quartz mainly depends on the heat transfer from other minerals instead of the electromagnetic dispersion.

4.1.4. Other minerals

As apparent in Fig. 10, the distribution of iron is the same as that of sulfur in the original shale. However, the distribution of sulfur in the microwave treated shale is similar to that of calcium. This implies that a related chemical reaction of pyrite and carbonate minerals occurs following the absorption of microwave. Minerals with low internal energy loss, such as quartz and feldspar (Zhou et al., 2011), are insensitive to microwave irradiation. Under microwave irradiation, such minerals would be penetrated by microwaves with little change in temperature. Thus, silicon, oxygen, potassium and aluminium all combine in a similar distribution before and after microwave simulation.

Densely distributed stomata are observed on calcite minerals in the microwaved shale (Fig. 11(d)). Calcite in the shale can be decomposed into calcium oxide and carbon dioxide at high temperature (Wang et al., 2016). The gas generated by the decomposition of calcite is responsible for the formation of pores in calcite minerals. The sulfur dioxide from pyrite oxidation and the calcium oxide from calcite decomposition react at high temperature to form sulfate minerals. Therefore, it can be seen from Figs. 10(b) and Fig. 11(c) that the distribution of calcium and sulfur is similar in the microwaved shale.

It can also be seen from the comparison between Fig. 11 (a) and

Fig. 11 (b) that the contours of quartz and calcium sulfite in the microwaved shale became clear and the pores and micro-fractures can be observed around these minerals. The narrow slits between most minerals in the original shale are often filled with clay minerals and organic carbon with compact combinations of minerals observed in Fig. 11 (a). The decomposition of organic carbon and clay minerals distributed between brittle minerals and stress caused by the uneven expansion of different minerals at microwave-induced high temperatures may be the possible causes of this phenomenon.

Based on the above analysis, the reasons of variations of temperature plateau, weight and pore structure with microwave irradiation are given. The temperature plateau is mainly due to the water evaporation (connate water in clay), mineral decomposition (e.g. decomposition of calcite) and mineral phase transition (e.g. α-β transition of quartz). The weight loss is due to the oxidation of organic matter generating gases. The increase of pore volume in shale after microwave irradiation mainly results from the pores generated by chemical reactions of mineral particles and the micro-cracks between mineral particles induced by thermal-stresses.

4.2. Microstructural characteristics of heating-induced micro-fractures in shale

The microstructure of the fractures for the original shale and that of the thermally-induced fractures developed across multiple bedding laminae for the microwaved shale are presented in Fig. 13 and Fig. 14, respectively. Compared to the tight cementation of minerals in the shale before microwaving, the minerals on the fracture surface for the microwaved shale are relatively fragmented and the accumulation between the minerals is relatively loose (Figs. 13 and 14).

The mechanism of the fracture induced by saturated vapor pressure in tight rock matrix are discussed in the work of Chen and his co-workers (Chen at al., 2018, 2021a) with that induced by differential thermal stress between distinct minerals presented in this work. The dielectric permittivity (imaginary part value of 12 at 25 °C and 2.45 GHz) (Liu et al., 2020) and thermal expansion coefficient (6.6×10^{-5} 1/K) (Jaeger et al., 2007) of water are much higher than minerals which listed in Table 2 and Fig. 10. For source rock samples with a moderate amount of pore-water, after microwave irradiation, the heating of water in the pores of matrix results in rapidly increased pore pressure. When the pressure exceeds the tensile strength of the rock, tension fractures will develop (Chen at al., 2018, 2021a). In this work, the different thermodynamic responses of different minerals after microwave treatment result in significant temperature differences between the minerals, leading to thermomechanical stresses. When this stress exceeds the compressive or tensile strength of the minerals, the mineral will rupture and transgranular fracture will ensue. The
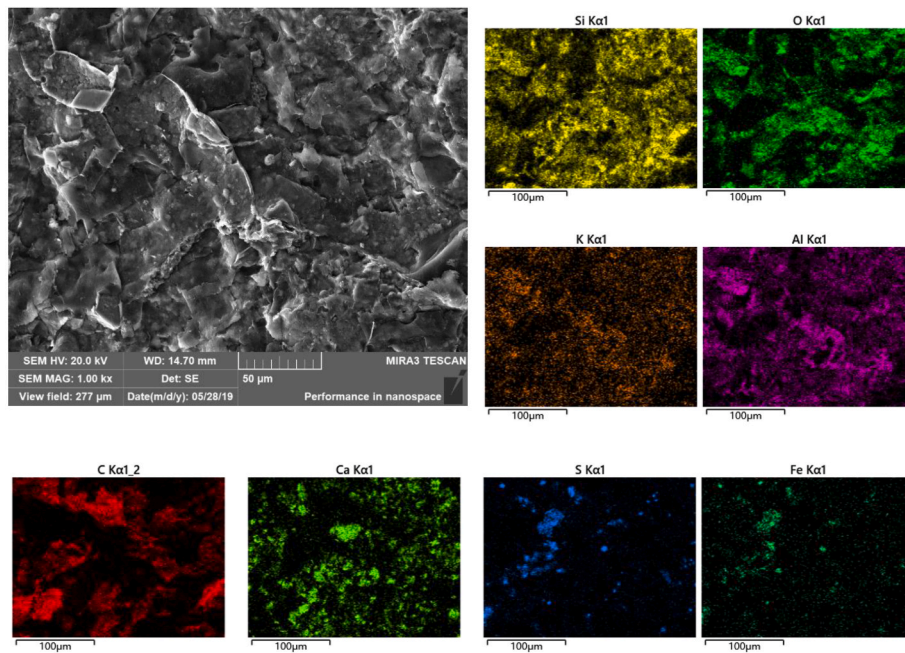
(a) The Microstructure and element distribution of organic matter enrichment area in unmicrowaved shale
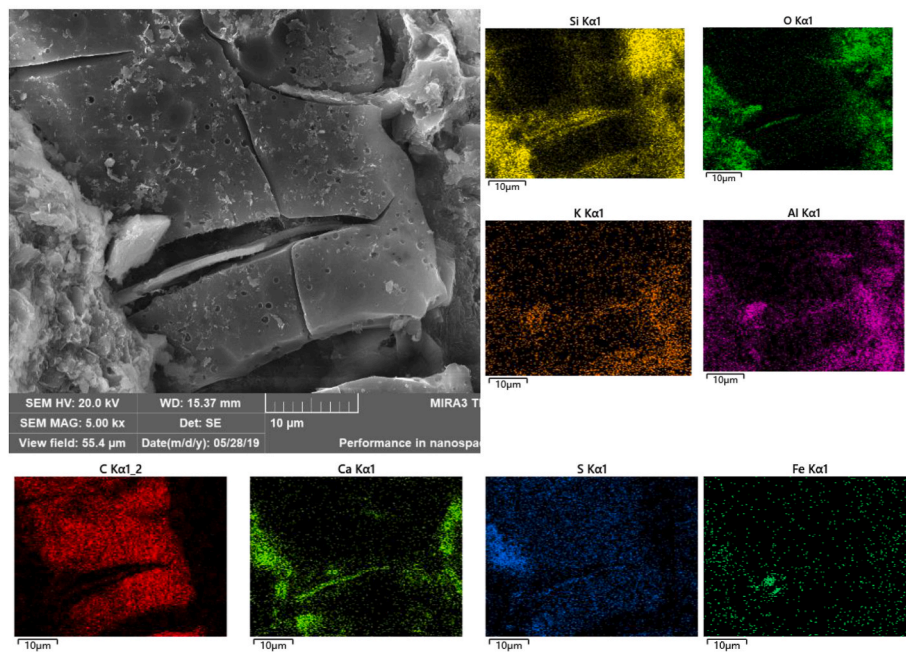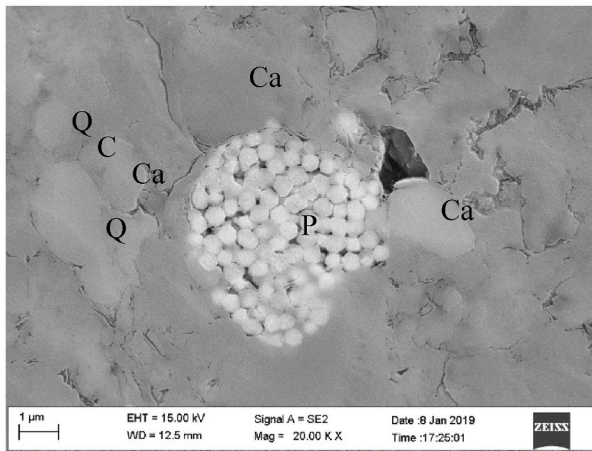

(b) The Microstructure and element distribution of organic matter enrichment area in microwaved shale

Fig. 10. Evolution of microstructure and elemental distribution of organic matter enrichment in un-microwave and microwave irradiated shale.

microwave-absorption-induced heat will cause thermal expansion of minerals. The degree of thermal expansion is directly related to the thermal expansion coefficient of the minerals. When the tensile or shear stress caused by the uncoordinated expansion and deformation of different minerals exceeds the bonding force between minerals, inter-granular fractures will appear.

The intercrystalline fracture can be observed between the microwave-induced products of calcite, pyrite and quartz (Fig. 14 (a), (b) and (e)). The strength of the mineral affects the development of the heat-induced fracture. Brittle minerals, such as quartz and feldspar, may undergo transgranular and intergranular fracturing at microwave-induced high temperatures (Fig. 14 (a) and (d)). The strength of clay minerals is lower than that of hard brittle minerals, thus, the main failure in the clays caused by thermal stress is by intercrystalline fracture (Fig. 14 (b) and (e)). It can also be seen from Fig. 14 (d) that the fracture surfaces of quartz and feldspar are smooth, suggesting the brittle frac-turing characteristics of these two minerals. Conversely, the fracture surfaces of clay show the characteristics of ductile fracturing. The
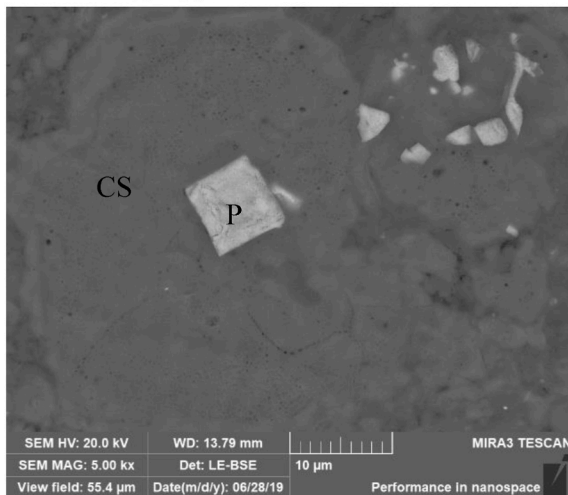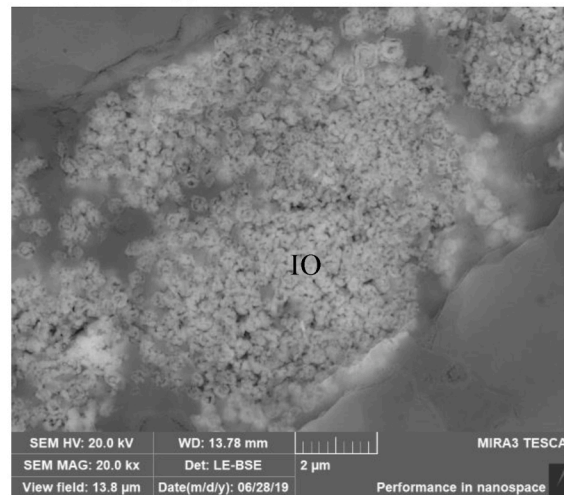
(a) Original shale.
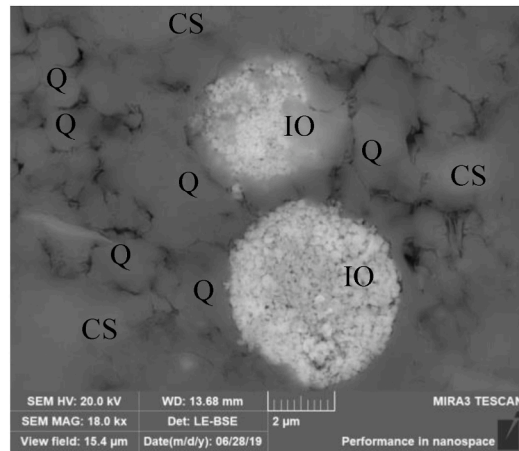
(b) Microwave irradiated shale.
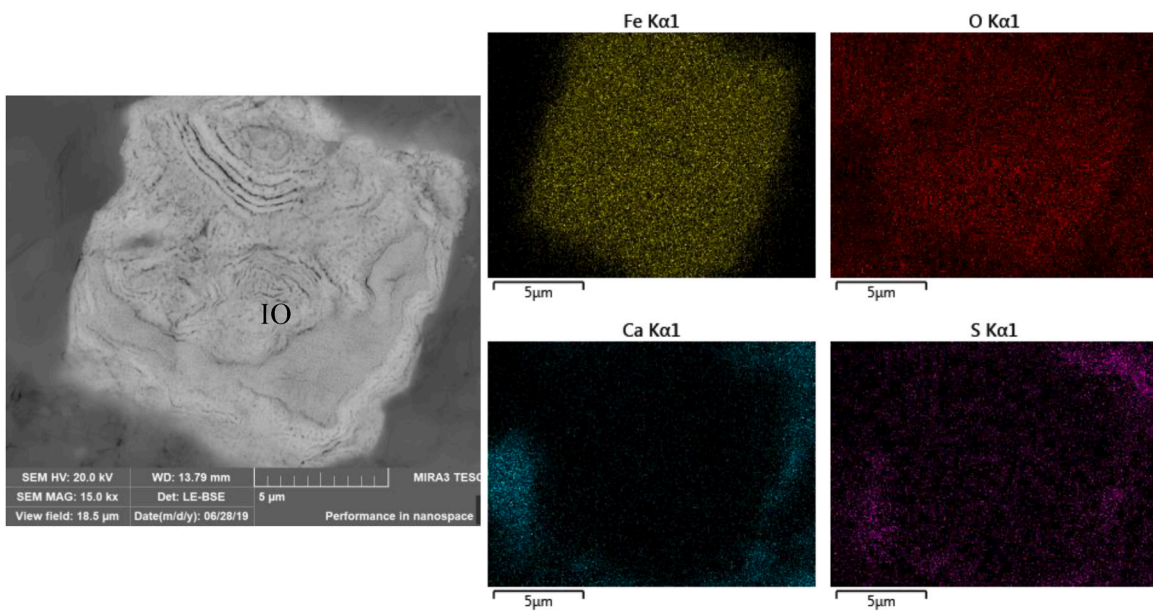
(c) Typical microstructure and elemental distribution of pyrite after oxidation.

(d) The pores in calcite minerals

(e) The new structures of the iron oxide

Fig. 11. Development of pore structure within the pyrite enrichment area in the shale induced by microwave stimulation (Ca: calcite, Q: quartz, P: pyrite, C: clay mineral, IO: Iron oxide, CS: calcium sulfite).
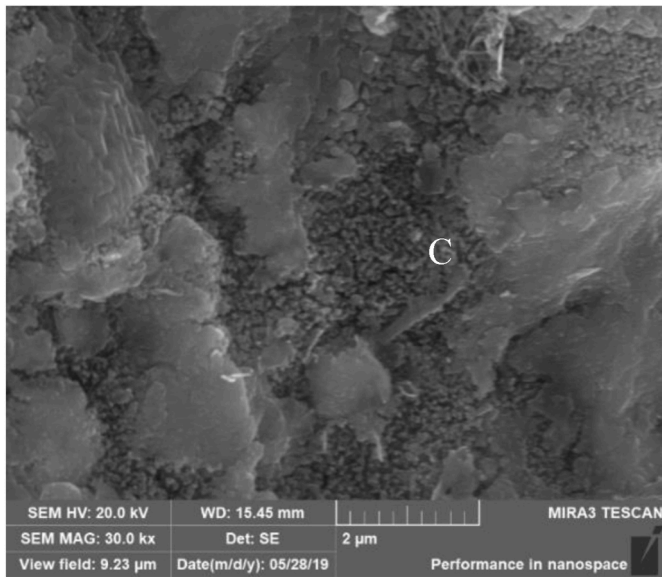
Fig. 12. The clay enrichment area in the shale after microwave stimulation.

chemical response of the mineral also affects the development of the heat-induced fracture. Due to the decomposition and oxidation of pyrite under microwave stimulation, tiny transgranular fractures develop in the originally dense particles of strawberry-shaped pyrite (Fig. 14(e) and (f)). Sulfate minerals produced by chemical reaction of calcite in shale following microwave heating has a new crystal structure, comprising many fine particles and nanopores (Fig. 14(e)).

As shown in the white box in Fig. 14(b) and (e), more traces of clay minerals being pulled apart can be observed on the thermal-fractures developed through multiple bedding planes for the microwaved shale. No evidence of shear is observed on the fracture surface of calcite and quartz, indicating that calcite and quartz are pulled apart by the tensile stress driven-by thermal expansion of the surrounding high-dielectric minerals. The above microstructural characteristics indicate that the thermal fractures crossing multiple sedimentary beddings result principally from the tensile failure of minerals.

Fig. 15 shows the microstructure of the thermally-induced fractures developed parallel and along bedding. No obvious tensile failure of the minerals can be observed. The bedding laminae appear first split by thermal stress and internal gas pressure from chemical reactions of some minerals in the early stages of microwave stimulation. The minerals on the surface of the bedding that rupture in the initial stage of microwave treatment will continue to chemically react at the even higher

temperatures caused by the subsequent microwave treatment, leading to further changes in the morphology of the fractures induced by tensile failure of the minerals.

Compared with the minerals on the thermally-induced fractures that transect multi-bedding-layers, the minerals (especially clay minerals and pyrite) on the surface of thermally-induced fractures developed along the bedding are exposed to microwave for a longer time, resulting in a more intense response to this exposure. Residual thin fragments of clay are left after this decomposition. The iron oxide particles formed on the thermally-induced fractures developed along the bedding are more broken than those transecting multiple layers of bedding (Fig. 15(d)). Areas rich in Fe, O, Si and Al may represent mixed particles from the products from high-temperature reaction and decomposition of pyrite and clay (the white box in Fig. 15(b)). The mineral particles in this region are loose, with localized pores and small cracks present in high density around these particles.

4.3. The effect of microwave heating on the anisotropic coefficients of permeability

Fig. 16 shows the coefficients of anisotropic shale permeability both before and after microwave irradiation. The ratio of the shale permeability parallel to bedding relative to that perpendicular to bedding is defined as the coefficient of anisotropic permeability. When the effective stress increases from 2.5 to 59.5 MPa, the coefficient of anisotropic permeability of the shale without microwave treatment decrease from 1.93 to 1.32 for the second loading cycle. At an effective stress of 2.5 MPa, the coefficient of anisotropic permeability for the shale after 690s, 1320s and 1650s of microwave irradiation are 10.53, 45.13 and 42.12, respectively. Under an effective stress of 59.5 MPa, the coefficient of anisotropic permeability following microwave stimulation for 690s, 1320s and 1650s are 1.75, 7.34 and 16.48, respectively. Under the same effective stress, the coefficient of anisotropic permeability increases with an increase in the duration of microwave irradiation. The coefficient of anisotropic permeability increases by an order of magnitude after microwave irradiation for 1650s at an effective stress of 59.5 MPa. The cementation of bedding in the shale is relatively weak, and the main fracture induced by thermal stresses develops along the bedding following microwave irradiation. This increases the difference in permeability in the two orthogonal directions for the shale. The coefficient of anisotropic permeability decreases with an increase in effective stress, indicating dominance of the permeability developed parallel to bedding as stress decreases.

For an infinitely small area in the shale sample, it could be treated as the uniform heating and electromagnetism dissipation energy can be seen as homogeneous in three directions. While Young's modulus in the direction along the bedding direction is several times larger than that in
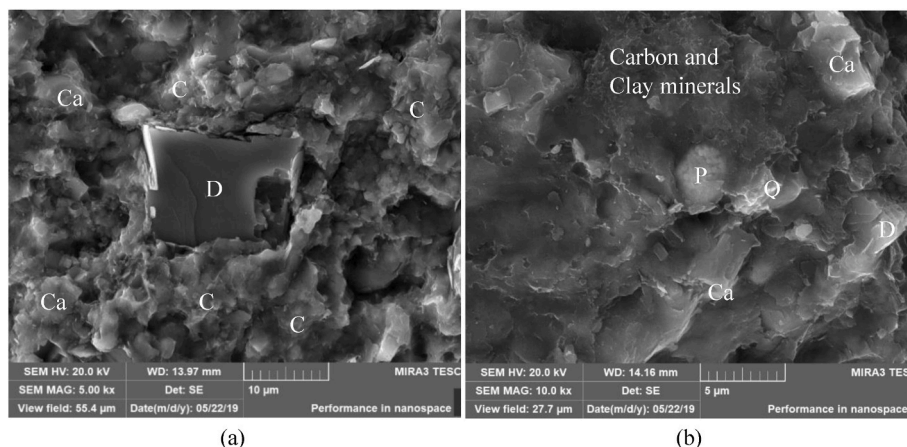

(a)   (b)

Fig. 13. Microstructure of the fractures in the original shale (Ca: calcite, D: dolomite, Q: quartz, P: pyrite, C: clay mineral).
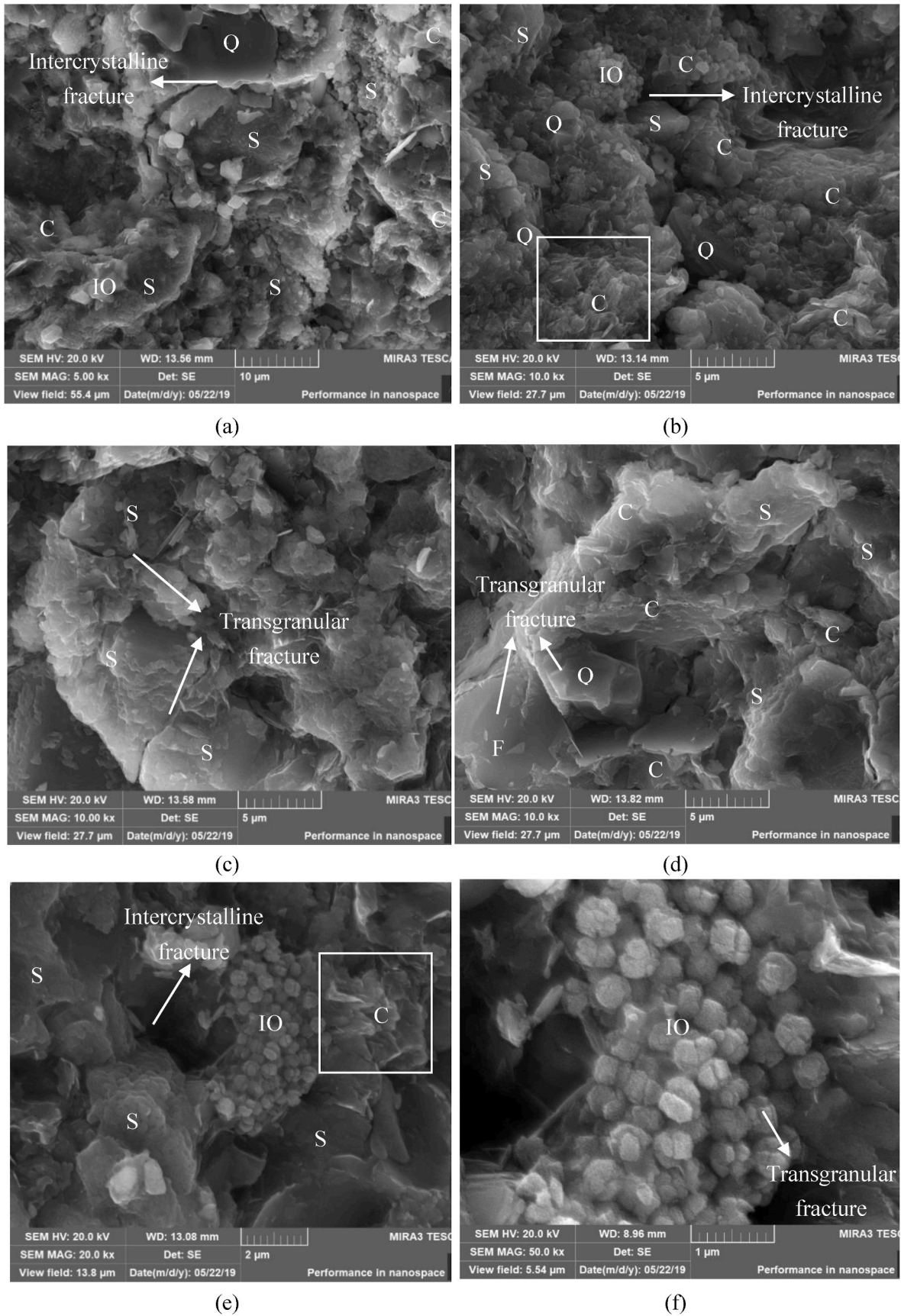
Fig. 14. Microstructure of thermally-induced fractures developed across multiple bedding planes (Q: quartz, F: feldspar, C: clay mineral, IO: Iron oxide, S: sulfate minerals).
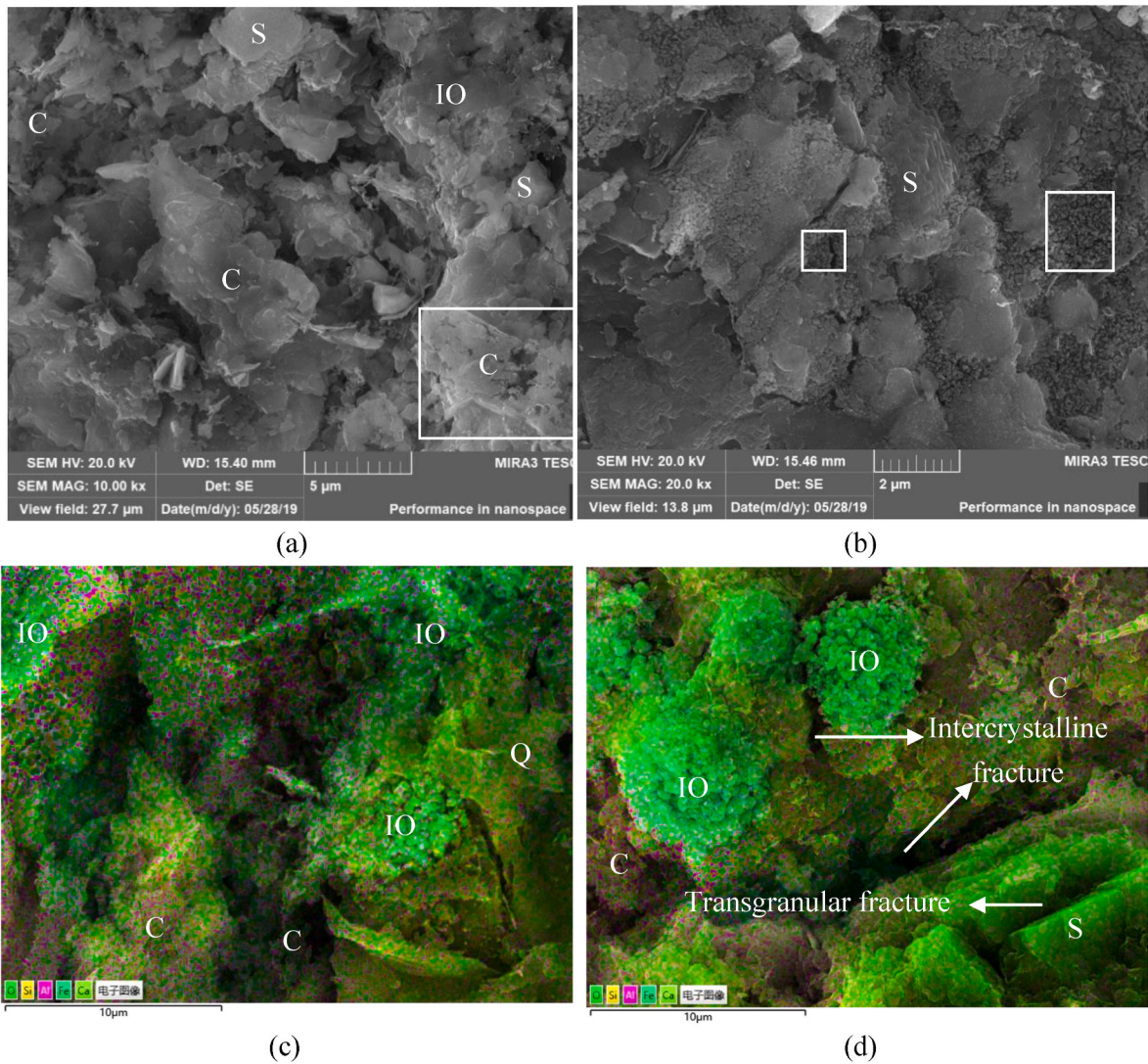
Fig. 15. Microstructure of the thermally-induced fractures developed along the bedding planes.
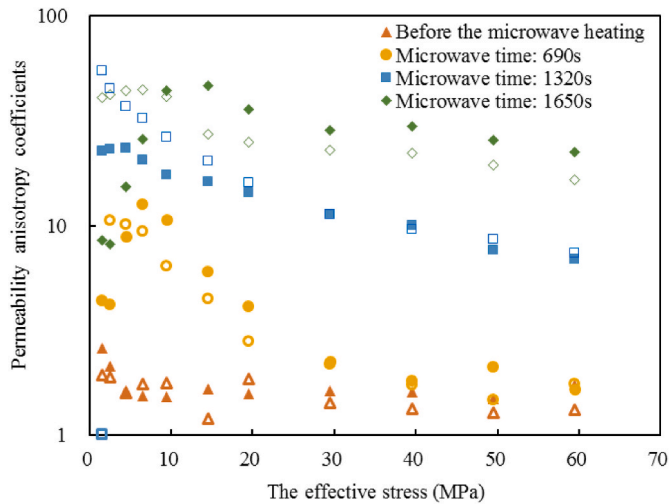

Fig. 16. Anisotropic coefficients of shale permeability both before and after microwave treatment (Solid symbols: anisotropic coefficients of shale permeability for the first loading cycle, Hollow symbols: anisotropic coefficients of shale permeability for the second loading cycle).

the perpendicular direction. Therefore the swelling deformation in the direction perpendicular to the bedding direction is larger than that in the direction along the bedding direction. Furthermore the permeability in one specific direction is defined as the function of the aperture of the fracture oriented in that direction which is pirated on by the swelling deformation perpendicular to that direction (Cui et al., 2019). Therefore, the permeability enhancement in the direction parallel to the bedding direction is larger than that in the direction perpendicular to the bedding direction. Besides that, once the tension stress exceeds the maximum tension strength, the rock would be damaged (Jones et al., 2005). The Brazilian split tests showed that when the bedding layer was perpendicular to the loading direction, the tensile strength reached its peak value, while when the bedding layer was parallel to the axial force direction, the minimum limit of tensile strength was obtained (Mokhtari et al., 2014; Vervoort et al., 2014). Therefore, the damage induced fracture may be firstly appeared along the bedding direction increasing the permeability coefficient of anisotropic permeability.

4.4. The compressibility of microwave-induced fracture

Fracture compressibility is often taken as a constant over a given range of stresses – but for shale it is typically highly nonlinear (Chen et al., 2021b). Fracture compressibility is rarely constant but stress-dependent when the range of effective stress change is large (Chen

et al., 2015a; Tan et al., 2019). An exponential relationship may be applied between permeability and stress with a stress-dependent fracture compressibility model used to fit the experimental data. Since the first series of data for each stress-loading case are obtained under the unconsolidated condition, these data are not used in the modeling.

An exponential relationship is usually applied to illustrate the dependence of permeability with stress for fractured reservoirs (McKee et al., 1988; Seidle et al., 1992):

$$k = k_0 e^{-3C_f(\sigma-\sigma_0)} \tag{5}$$

in which k denotes the permeability value at effective stress σ, σ_0 and k_0 is the initial permeability and effective stress, respectively, and C_f is fracture compressibility.

A mean compressibility $\overline{C_f}$ is introduced to replace C_f in Eq. (5) with the assumption that the fracture compressibility decreases exponentially as effective stress increases McKee et al. (1988):

$$\overline{C_f} = \frac{C_{f0}}{\alpha(\sigma-\sigma_0)}\left(1 - e^{-\alpha(\sigma-\sigma_0)}\right) \tag{6}$$

in which $\overline{C_f}$ denotes the average compressibility when the stress decreases from σ to σ_0; C_{f0} and σ_0 is an initial compressibility and effective stress, respectively; and α is the decline rate of pore compressibility with increasing effective stress.

Applying Eq. (6) into Eq. (5), yields:

$$k = k_0 e^{-3\frac{C_{f0}}{\alpha(\sigma-\sigma_0)}\left(1-e^{-\alpha(\sigma-\sigma_0)}\right)(\sigma-\sigma_0)} \tag{7}$$

To obtain the compressibility of the thermally-induced fracture under the microwave irradiation applied in this work, the experimental data of permeability versus effective stress were fit to Eq. (7). An initial reference effective stress σ_0 is assumed as 0 MPa in the following. The modeling results with Eq. (7) for the parameters are listed in Fig. 17. The mean compressibilities of the Longmaxi shale samples, for the second loading cycle, range from 0.12 to 0.014 MPa^{-1} before microwave treatment as the effective stresses increase from 1.5 to 59.5 MPa. The range of compressibilities change to 0.14 to 0.027 MPa^{-1} over the same stress range after microwave treatment. The increase in shale compressibility due to microwave irradiation results from microwave-induced fracturing. The shale compressibility first increases and then decreases during the process of microwave stimulation. During the initial phase of microwave irradiation, the number and size of fractures induced by the thermal stress increase gradually with the increasing duration of microwave heating – increasing fracture compressibility. When the microwave irradiation ceases, the fractures generated in the
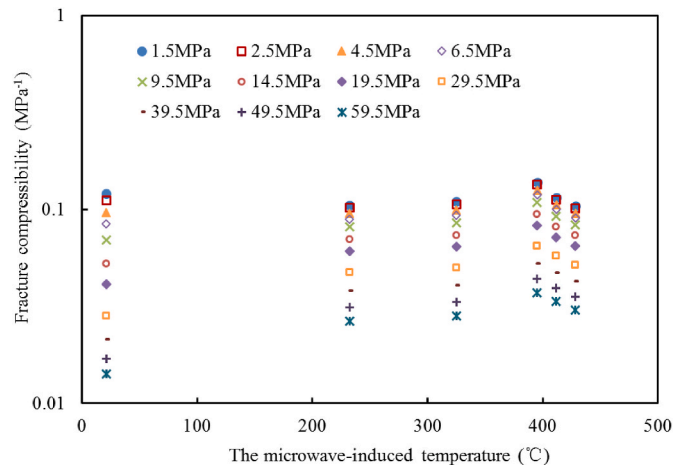
initial stage of microwave irradiation will gradually close with the decrease in sample temperature. Nevertheless, after a certain period of microwave treatment, even at room temperature, the heating-induced fractures will remain open, due to the incremental increase in damage to the surface. The minerals present on the heating-induced fracture surface will continue to decompose under the subsequent microwave action, leading to changes in the roughness and stiffness of the fracture surface - potentially one of the reasons why the microwave-induced fractures remain open. The enhancement of fracture plasticity and damage and the change in roughness and stiffness are the key reasons for the decrease in fracture compressibility in the later stages of microwave heating.

4.5. Implications of microwave heating to the field application

For the reservoir application, the penetration depth (D_p) should be considered as the amplitude of microwave diminishes when penetrating into a material. D_p is written as (Liu et al., 2018a):

$$D_p = \frac{C}{2\pi f\sqrt{2\varepsilon_r}\left(\sqrt{1 + \tan^2\left(\frac{\varepsilon_i}{\varepsilon_r}\right)} - 1\right)^{1/2}} \tag{8}$$

where C is the speed of light, f is the frequency, ε_r is the real part of the relative permittivity, ε_i denotes the imaginary part; D_p in shale is on a scale of meters because of the low ε_r of shale matrix (Liu et al., 2018a). As observed in Eq. (8), reducing frequency is common to enhance D_p. For the heating path, the intermittent microwave irradiation (IMI) is strongly suggested based on the experiment results in this work.

Once combined with fracturing methods such as hydrofracturing, microwave can heat the shale reservoir and a series of chemical and mechanic interactions would occur at different scales. (1) At the mineral scale, (i) the organic matter inside the shale can heat up rapidly after microwave stimulation, and some kerogen rapidly absorbs heat and releases natural gas; (ii) the microwave irradiation would increase the number of pores with a diameter less than 130 nm and therefore enhance the diffusion in the shale matrix (Cui et al., 2020c). (2) At the micro-scale, (i) the transgranular and intergranular fracture at microwave-induced high temperatures are both occurred in the brittle minerals, (ii) intercrystalline fracture can be observed between the microwave-induced products of calcite, pyrite and quartz. (3) At macro-scale as proved in this work, (i) the heating-induced fractures first appear along the bedding then perpendicular to the bedding direction; (ii) microwave treatment mainly promotes an increase in permeability parallel to the bedding direction; (iii) shale fracture compressibility first increases and then decreases during the process of microwave stimulation.

5. Conclusions

This work explored the feasibility of microwave heating fracturing for enhanced shale gas recovery. The effects of continuous and intermittent microwave heating on the initiation and development of thermal-induced fractures in shale were investigated. The effects of microwave irradiation on the permeability of two shale samples at different effective stresses were analyzed. The microstructure and mineral composition of the shale after microwave irradiation were investigated by SEM-EDS. A permeability model considering the changing of effective stresses was applied to fit the experimental data. The effects of microwave irradiation on fracture compressibility and permeability anisotropy for the shale were also investigated. The following conclusions are drawn:

1. The value of temperature of 400 °C is a critical value. Loss rates of shale weight increase rapidly while the temperature reaches a plateau at this temperature. The former term is due to the oxidation

Fig. 17. Fracture compressibility of both original and microwave treated shales.

of organic matter generating gases. The temperature plateau is mainly because of the water evaporation (connate water in clay), mineral decomposition (e.g. decomposition of calcite) and mineral phase transition (e.g. α-β transition of quartz).

2. The preferred pathway for microwave fracturing of shale matrix is the intermittent microwave irradiation pathway as found in this work. Continuous microwave irradiation results in the more rapid rise of temperature, the thermally-induced stresses and chemically-induced gas pressures compared to intermittent irradiation, eventually resulting in the fragmentation of the shale. While the shale treated under intermittent microwave irradiation withstands the microwave irradiation without fragmentation, enabling the complex heating-induced fracture network.

3. Under microwave irradiation, fractures and pores develop in the shale due to thermally-induced stresses and chemical-transformation-induced gas pressures. The porosity of the studied shale increased from 1.57% to 3.83% with the pores of diameters less than 130 nm taking the dominant role due to the oxidation of organic matter and pyrite, and decomposition of clay minerals and calcite. Thermomechanical stresses induced fractures across multiple sedimentary bedding planes - mainly resulting from thermally-induced tensile failure, and chemical transformations control the heating-induced fractures that develop along the bedding. Brittle minerals undergo both transgranular and intergranular fracture: the destruction of clay minerals is manifest more commonly as transgranular fracture.

4. Increases in shale permeability are positively correlated with the duration of microwave irradiation and temperature increment. The shale permeability increases rapidly when the temperature value is above 325 °C, indicating that when the temperature is above a certain threshold, the fractures and pores develop rapidly. On the other hand, the enhanced permeability is highly sensitive to effective stress increment.

5. The microwave treatment accentuates permeability anisotropy because that the damage induced fractures are easily appeared along the bedding direction; The shale compressibility first increases and then decreases during microwave irradiation. The appearance of fractures induced by the thermal stress during the early stage increase fracture compressibility. The enhancement of fracture plasticity and damage, and the change in roughness and stiffness are the main contributors to the decrease in the later stage.

Declaration of competing interest

The authors declare that they have no known competing financial interests or personal relationships that could have appeared to influence the work reported in this paper.
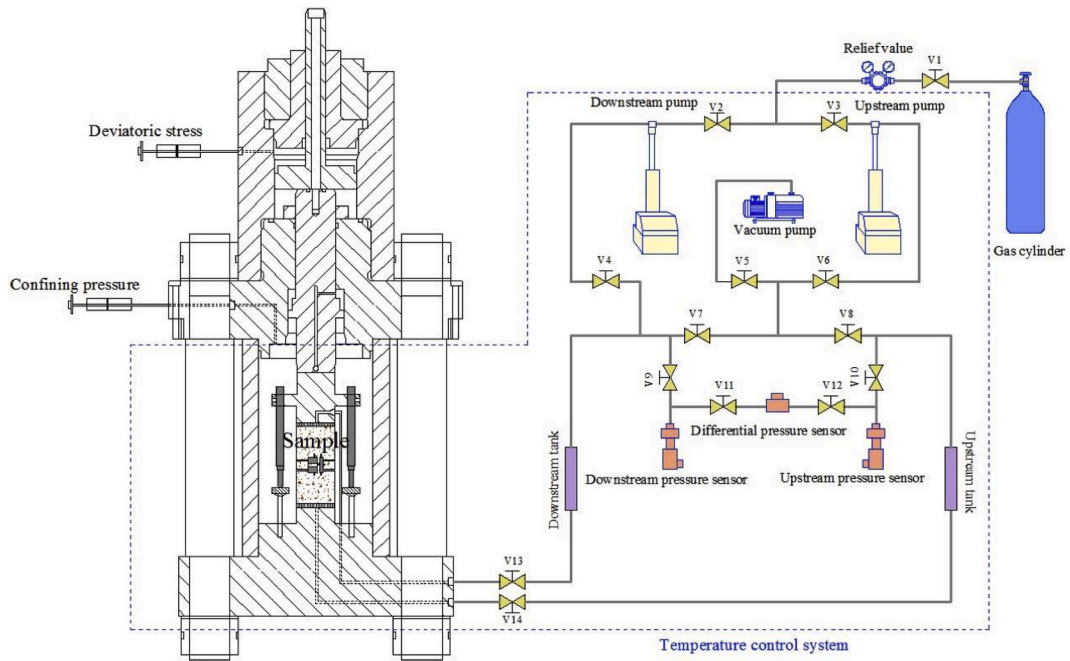
Acknowledgment

Appendix A

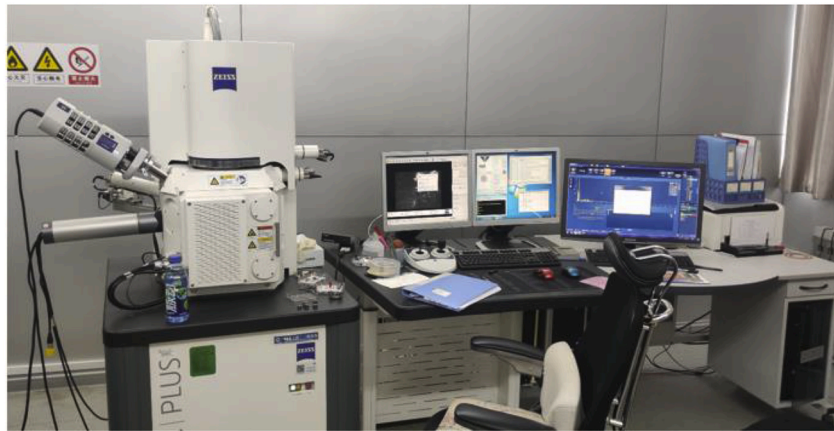**Fig. A.1.** Image of microwave oven.

(a) Schematic diagram

(b) Photo

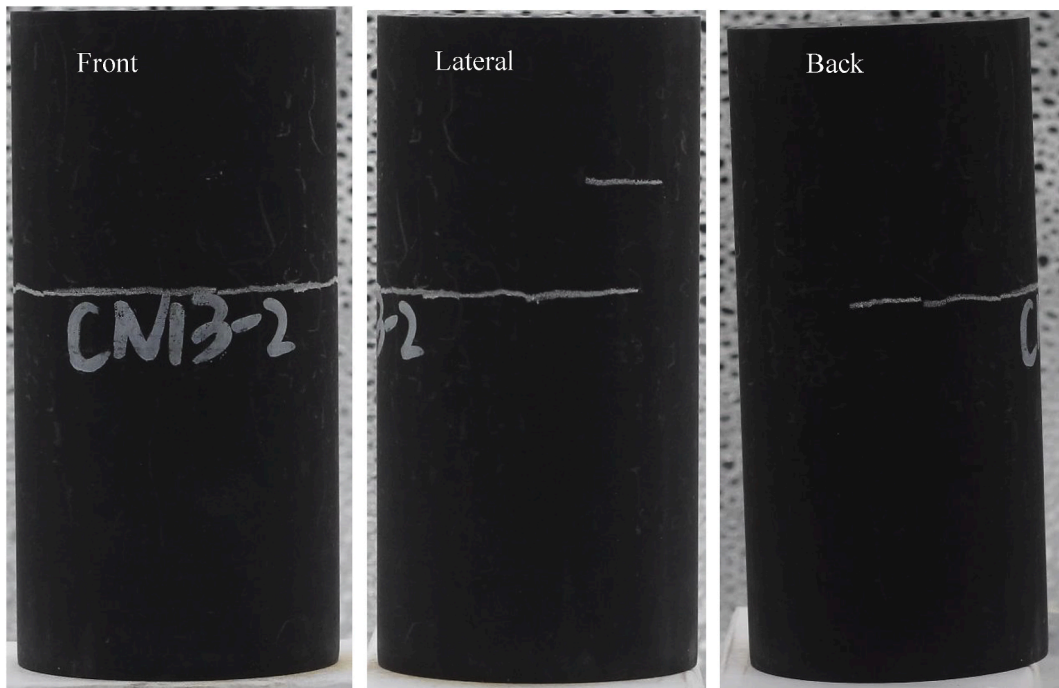**Fig. A.2.** Image of multi-physics coupling testing system.

TESCAN MIRA 3 XMU

ZEISS ULTRA PLUS

Fig. A.3. Image of Scanning electron microscope.

(a) 150s

(b) 420s

Fig. A.4. Shale samples with flow-perpendicular bedding after intermittent microwave treatment.
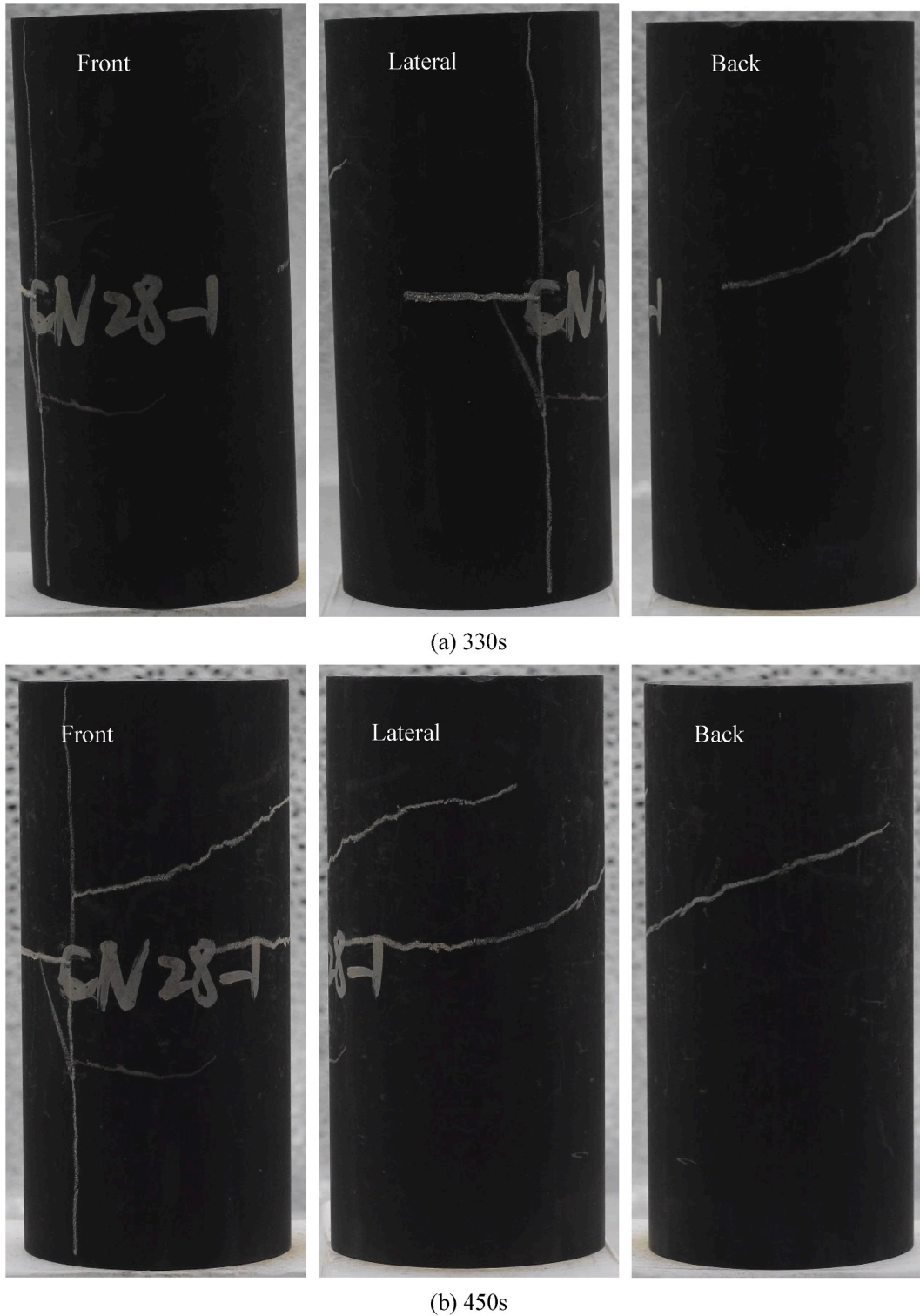
(a) 330s

(b) 450s

Fig. A.5. Shale samples with flow-parallel bedding after intermittent microwave treatment.

References

Aqil, S., Schmitt, D.R., 2010. Dielectric permittivity of clay adsorbed water: effect of salinity. GeoConvention 2010 1–4.

Bientinesi, M., Petarca, L., Cerutti, A., Bandinelli, M., De Simoni, M., Manotti, M., Maddinelli, G., 2013. A radiofrequency/microwave heating method for thermal heavy oil recovery based on a novel tight-shell conceptual design. J. Petrol. Sci. Eng. 107, 18–30.

Boudet, H., Clarke, C., Bugden, D., Maibach, E., Roser-Renouf, C., Leiserowitz, A., 2014. "Fracking" controversy and communication: using national survey data to understand public perceptions of hydraulic fracturing. Energy Pol. 65, 57–67.

Brace, W.F., Walsh, J.B., Frangos, W.T., 1968. Permeability of granite under high pressure. J. Geophys. Res. 73 (6), 2225–2236.

Carrol, D., 1970. Clay Minerals: a Guide to Their X-Ray Identification. Geological Society of America, p. 75 special paper 126.

Chen, D., Pan, Z., Ye, Z., 2015a. Dependence of gas shale fracture permeability on effective stress and reservoir pressure: model match and insights. Fuel 139, 383–392.

Chen, J.-H., Althaus, S.M., Liu, H.-H., Zhang, J., Eppler, G., Duncan, J.C., Sun, Q., 2021a. Electromagnetic-heating enhancement of source rock permeability for high recovery. Fuel 283, 118976.

Chen, J.-H., Georgi, D.T., Liu, H.-H., 2018. Electromagnetic thermal stimulation of shale reservoirs for petroleum production. J. Nat. Gas Sci. Eng. 59, 183–192.

Chen, T., Feng, X.-T., Cui, G., Tan, Y., Pan, Z., 2019. Experimental study of permeability change of organic-rich gas shales under high effective stress. J. Nat. Gas Sci. Eng. 64, 1–14.

Chen, T., Feng, X.-T., Tan, Y., Cui, G., Elsworth, D., Pan, Z., 2021b. Gas permeability and fracture compressibility for proppant-supported shale fractures under high stress. J Nat Gas Sci Eng, under review.

Chen, T., Feng, X.T., Pan, Z., 2015b. Experimental study of swelling of organic rich shale in methane. Int. J. Coal Geol. 150–151, 64–73.

Chen, W., Lei, Y., Ma, L., Yang, L., 2017. Experimental study of high temperature combustion for enhanced shale gas recovery. Energy Fuel. 31 (9), 10003–10010.

Church, R.H., Webb, W.E., Salsman, J., 1988. Dielectric Properties of Low-Loss Minerals.

Cui, G., Chen, T., Feng, X., Chen, Z., Elsworth, D., Yu, H., Zheng, X., Pan, Z., 2020a. Coupled multiscale-modeling of microwave-heating-induced fracturing in shales. Int J Rock Mech Min 136, 104520.

Cui, G., Liu, J., Wei, M., Feng, X., Elsworth, D., 2018. Evolution of permeability during the process of shale gas extraction. J. Nat. Gas Sci. Eng. 49, 94–109.

Cui, G., Tan, Y., Chen, T., Feng, X.-T., Elsworth, D., Pan, Z., Wang, C., 2020b. Multidomain two-phase flow model to study the impacts of hydraulic fracturing on shale gas production. Energy Fuel. 34 (4), 4273–4288.

Cui, G., Wei, J., Feng, X.-T., Liu, J., Elsworth, D., Chen, T., Xiong, W., 2019. Preliminary study on the feasibility of co-exploitation of coal and uranium. Int J Rock Mech Min 123, 104098.

Cui, G., Xia-Ting, F., Pan, Z., Chen, T., Liu, J., Elsworth, D., Tan, Y., Wang, C., 2020c. Impact of shale matrix mechanical interactions on gas transport during production. J. Petrol. Sci. Eng. 184, 106524.

Flesoura, G., Garcia-Banos, B., Catala-Civera, J.M., Vleugels, J., Pontikes, Y., 2019. In-situ measurements of high-temperature dielectric properties of municipal solid waste incinerator bottom ash. Ceram. Int. 45 (15), 18751–18759.

Ge, L., Zhang, Y., Wang, Z., Zhou, J., Cen, K., 2013. Effects of microwave irradiation treatment on physicochemical characteristics of Chinese low-rank coals. Energy Convers. Manag. 71, 84–91.

Han, X., Liu, Q., Jiang, X., 2015. Heat transfer characteristic of oil shale particle during the retorting. Int. J. Heat Mass Tran. 84, 578–583.

Hartlieb, P., Toifl, M., Kuchar, F., Meisels, R., Antretter, T., 2016. Thermo-physical properties of selected hard rocks and their relation to microwave-assisted comminution. Miner. Eng. 91, 34–41.

Hong, Y.-d., Lin, B.-q., Zhu, C.-j., Li, H., 2016. Effect of microwave irradiation on petrophysical characterization of coals. Appl. Therm. Eng. 102, 1109–1125.

Huang, J., Hu, G., Xu, G., Nie, B., Yang, N., Xu, J., 2019. The development of microstructure of coal by microwave irradiation stimulation. J. Nat. Gas Sci. Eng. 66, 86–95.

Jaeger, J.C., Cook, N.G.W., Zimmerman, R., 2007. Fundamentals of Rock Mechanics. Wiley.

Jiang, X., Han, X., Cui, Z., 2007. Progress and recent utilization trends in combustion of Chinese oil shale. Prog Energ Combust 33 (6), 552–579.

Jones, D.A., 2005. Understanding Microwave Treatment of Ores. Doctor. University of Nottingham.

Jones, D.A., Kingman, S., Whittles, D., Lowndes, I., 2005. Understanding microwave assisted breakage. Miner. Eng. 18 (7), 659–669.

Jones, D.A., Kingman, S.W., Whittles, D.N., Lowndes, I.S., 2007. The influence of microwave energy delivery method on strength reduction in ore samples. Chem. Eng. Process 46 (4), 291–299.

Josh, M., Clennell, B., 2015. Broadband electrical properties of clays and shales: comparative investigations of remolded and preserved samplesBroadband electrical properties of clay. Gophysics 80 (2), D129–D143.

Kang, Y., Chen, M., Chen, Z., You, L., Hao, Z., 2016. Investigation of formation heat treatment to enhance the multiscale gas transport ability of shale. J. Nat. Gas Sci. Eng. 35, 265–275.

Kasevich, R.S., 2008. Method and Apparatus for In-Situ Radiofrequency Assisted Gravity Drainage of Oil (USA).

Li, H., Lin, B., Yang, W., Zheng, C., Hong, Y., Gao, Y., Liu, T., Wu, S., 2016. Experimental study on the petrophysical variation of different rank coals with microwave treatment. Int. J. Coal Geol. 154–155, 82–91.

Li, H., Shi, S., Lin, B., Lu, J., Lu, Y., Ye, Q., Wang, Z., Hong, Y., Zhu, X., 2019. A fully coupled electromagnetic, heat transfer and multiphase porous media model for microwave heating of coal. Fuel Process Tchnol 189, 49–61.

Liu, J.-Z., Zhu, J.-F., Cheng, J., Zhou, J.-H., Cen, K.-F., 2015. Pore structure and fractal analysis of Ximeng lignite under microwave irradiation. Fuel 146, 41–50.

Liu, J., Liang, X., Xue, Y., Yao, K., Fu, Y., 2020. Numerical evaluation on multiphase flow and heat transfer during thermal stimulation enhanced shale gas recovery. Appl. Therm. Eng. 178, 115554.

Liu, J., Wang, J., Leung, C., Gao, F., 2018. A fully coupled numerical model for microwave heating enhanced shale gas recovery. Energies 11 (6), 1608.

Lovás, M., Kováčová, M., Dimitrakis, G., Čuvanová, S., Znamenáčková, I., Jakabský, Š., 2010. Modeling of microwave heating of andesite and minerals. Int. J. Heat Mass Tran. 53 (17–18), 3387–3393.

McKee, C.R., Bumb, A.C., Koenig, R.A., 1988. Stress-dependent permeability and porosity of coal and other geologic formations. SPE Form. Eval. 3 (1), 81–91.

Meisels, R., Toifl, M., Hartlieb, P., Kuchar, F., Antretter, T., 2015. Microwave propagation and absorption and its thermo-mechanical consequences in heterogeneous rocks. Int. J. Miner. Process. 135, 40–51.

Mokhtari, M., Bui, B., Tutuncu, A., 2014. Tensile Failure of Shales: Impacts of Layering and Natural Fractures. Society of Petroleum Engineers Western North America and Rocky Mountain Joint Conference and Exhibition 2014.

Mutyala, S., Fairbridge, C., Paré, J.R.J., Bélanger, J.M.R., Ng, S., Hawkins, R., 2010. Microwave applications to oil sands and petroleum: a review. Fuel Process. Technol. 91 (2), 127–135.

Rui, Z., Wang, X., Zhang, Z., Lu, J., Chen, G., Zhou, X., Patil, S., 2018. A realistic and integrated model for evaluating oil sands development with Steam Assisted Gravity Drainage technology in Canada. Appl. Energy 213, 76–91.

Sahoo, B.K., De, S., Meikap, B.C., 2011. Improvement of grinding characteristics of Indian coal by microwave pre-treatment. Fuel Process. Technol. 92 (10), 1920–1928.

Salvi, D., Boldor, D., Ortego, J., Aita, G.M., Sabliov, C.M., 2010. Numerical modeling of continuous flow microwave heating: a critical comparison of COMSOL and ANSYS. J Microwave Power EE 44 (4), 187–197.

Seehra, M., Kalra, A., Manivannan, A., 2007. Dewatering of fine coal slurries by selective heating with microwaves. Fuel 86 (5–6), 829–834.

Seidle, J.P., Jeansonne, M.W., Erickson, D.J., 1992. Application of matchstick geometry to stress dependent permeability in coals. In: SPE Rocky Mountain Regional Meeting. Casper, Wyoming. Society of Petroleum Engineers.

Skauge, A., Fuller, N., Hepler, L.G., 1983. Specific heats of clay minerals: sodium and calcium kaolinites, sodium and calcium montmorillonites, illite, and attapulgite. Thermochim Acat 61 (1), 139–145.

Tan, Y., Pan, Z., Feng, X.-T., Zhang, D., Connell, L.D., Li, S., 2019. Laboratory characterisation of fracture compressibility for coal and shale gas reservoir rocks: a review. Int. J. Coal Geol. 204, 1–17.

Tan, Y., Pan, Z., Liu, J., Feng, X.-T., Connell, L.D., 2018. Laboratory study of proppant on shale fracture permeability and compressibility. Fuel 222, 83–97.

Toifl, M., Hartlieb, P., Meisels, R., Antretter, T., Kuchar, F., 2017. Numerical study of the influence of irradiation parameters on the microwave-induced stresses in granite. Miner. Eng. 103–104, 78–92.

Vervoort, A., Min, K.B., Konietzky, H., Cho, J.W., Debecker, B., Dinh, Q.D., Frühwirt, T., Tavallali, A., 2014. Failure of transversely isotropic rock under Brazilian test conditions. Int J Rock Mech Min 70, 343–352.

Wang, H., Rezaee, R., Saeedi, A., 2015. The interaction of reservoir properties and microwave heating – an experimental and numerical modelling study of enhanced gas recovery (EGR). Procedia Earth and Planetary Science 15, 542–548.

Wang, H., Rezaee, R., Saeedi, A., 2016. Preliminary study of improving reservoir quality of tight gas sands in the near wellbore region by microwave heating. J. Nat. Gas Sci. Eng. 32, 395–406.

Wang, H., Rezaee, R., Saeedi, A., Josh, M., 2017. Numerical modelling of microwave heating treatment for tight gas sand reservoirs. J. Petrol. Sci. Eng. 152, 495–504.

Wang, H., Wang, J.G., Wang, X., Dou, F., 2019a. Interaction of shale gas recovery and moisture transport in post two-phase flowback stage. J. Nat. Gas Sci. Eng. 68, 102897.

Wang, L., Chen, Z., Wang, C., Elsworth, D., Liu, W., 2019b. Reassessment of coal permeability evolution using steady-state flow methods: the role of flow regime transition. Int. J. Coal Geol. 211, 103210.

Wang, Y., Djordjevic, N., 2014. Thermal stress FEM analysis of rock with microwave energy. Int. J. Miner. Process. 130, 74–81.

Xu, C., Kang, Y., You, Z., Chen, M., 2016. Review on formation damage mechanisms and processes in shale gas reservoir: known and to be known. J. Nat. Gas Sci. Eng. 36, 1208–1219.

Yang, Z., Zhu, J., Li, X., Luo, D., Qi, S., Jia, M., 2017. Experimental investigation of the transformation of oil shale with fracturing fluids under microwave heating in the presence of nanoparticles. Energy Fuel. 31 (10), 10348–10357.

Youjun, J., 2017. Analysis of pore scale migration in a porous medium- application to coal rock seam. Int J Numer Method H 27 (8), 1706–1719.

Zhang, J., Zhu, D., Hill, A.D., 2015. Water-induced fracture conductivity damage in shale formations. In: SPE Hydraulic Fracturing Technology Conference. Society of Petroleum Engineers, The Woodlands, Texas, USA.

Zheng, Y., Wang, S., Feng, J., Ouyang, Z., Li, X., 2005. Measurement of the complex permittivity of dry rocks and minerals: application of polythene dilution method and Lichtenecker's mixture formulae. Geophys. J. Int. 163 (3), 1195–1202.

Zheng, Y.L., Zhang, Q.B., Zhao, J., 2017. Effect of microwave treatment on thermal and ultrasonic properties of gabbro. Appl. Therm. Eng. 127, 359–369.

Zhou, F., Cheng, J., Wang, A., Liu, J., Zhou, J., Cen, K., 2015. Upgrading Chinese Shengli lignite by microwave irradiation for slurribility improvement. Fuel 159, 909–916.

Zhou, Y., Li, E., Guo, G., Gao, Y., Yang, T., 2011. Broadband complex permittivity measurement of low loss materials over large temperature ranges by stripline resonator cavity using segmentation calculation method. Prog Electromagn Res 113, 143–169.

Zhu, G., Yao, J., Sun, H., Zhang, M., Xie, M., Sun, Z., Lu, T., 2016. The numerical simulation of thermal recovery based on hydraulic fracture heating technology in shale gas reservoir. J. Nat. Gas Sci. Eng. 28, 305–316.